

Summer 2019

Structural Studies of Complexes of Blood Coagulation Factor VIII

Joseph S. Gish

Western Washington University, mrjosephgish@gmail.com

Follow this and additional works at: <https://cedar.wvu.edu/wwuet>



Part of the [Chemistry Commons](#)

Recommended Citation

Gish, Joseph S., "Structural Studies of Complexes of Blood Coagulation Factor VIII" (2019). *WWU Graduate School Collection*. 902.
<https://cedar.wvu.edu/wwuet/902>

This Masters Thesis is brought to you for free and open access by the WWU Graduate and Undergraduate Scholarship at Western CEDAR. It has been accepted for inclusion in WWU Graduate School Collection by an authorized administrator of Western CEDAR. For more information, please contact westerncedar@wvu.edu.

STRUCTURAL STUDIES OF COMPLEXES OF BLOOD COAGULATION FACTOR VIII

By
Joseph S. Gish

Accepted in Partial Completion of the
Requirements for the Degree Master of Science

ADVISORY COMMITTEE

Chair, Dr. P. Clint Spiegel

Dr. Jeanine Amacher

Dr. Spencer Anthony-Cahill

GRADUATE SCHOOL

David L. Patrick
Interim Dean of the Graduate School

MASTER'S THESIS:

In presenting this thesis in partial fulfillment of the requirements for a master's degree at Western Washington University, I grant to Western Washington University the non-exclusive royalty-free right to archive, reproduce, distribute, and display the thesis in any and all forms, including electronic format, via any digital library mechanisms maintained by WWU.

I represent and warrant this is my original work, and does not infringe or violate any rights of others. I warrant that I have obtained written permissions from the owner of any third party copyrighted material included in these files.

I acknowledge that I retain ownership rights to the copyright of this work, including but not limited to the right to use all or part of this work in future works, such as articles or books.

Library users are granted permission for individual, research and non-commercial reproduction of this work for educational purposes only. Any further digital posting of this document requires specific permission from the author.

Any copying or publication of this thesis for commercial purposes, or for financial gain, is not allowed without my written permission.

Joseph S. Gish

August 13th, 2019

STRUCTURAL STUDIES OF COMPLEXES OF BLOOD COAGULATION FACTOR VIII

A Thesis Presented to
The Faculty of Western Washington University

Accepted in Partial Completion of the
Requirements for the Degree Master of Science

By
Joseph S. Gish
August 2019

Abstract

Factor VIII (FVIII) is a 2332 amino acid glycoprotein with domain organization of A1-A2-B-A3-C1-C2 which is a crucial component of the blood coagulation cascade. After secretion, FVIII circulates in the bloodstream at a concentration of one nanomolar bound to von Willebrand Factor (vWF) which protects FVIII from clearance. In the event of an injury to the bloodstream, FVIII is proteolytically cleaved, releases from vWF and binds to both activated platelet surfaces and activated Factor IX with nanomolar affinity. These interactions increase the rate of blood clot formation 100,000 fold. Hemophilia A is an x-linked recessive disease affecting 1 in 5000 males which is due to a deficiency of functional FVIII. Treatment involves prophylactically injecting FVIII into the bloodstream. Although this treatment works, the short half-life of FVIII demands multiple injections per week and nearly one-third of patients receiving treatment develop antibody inhibitors which target injected FVIII. This results in dramatically worse quality of life for hemophilia A patients. Greater understanding of the physiological role of FVIII in its interactions with vWF and inhibitor antibodies can lead to improved therapy by extending the half-life of engineered FVIII therapeutics and reducing immunogenicity. Towards this end, FVIII chimeric variant Et3i was co-crystallized in two different complexes. Et3i is a B-domain deleted chimera consisting of porcine A1 and A3 domains and human A2, C1 and C2 domains. The first structure was with the antigen binding fragment of murine inhibitory antibody 2A9 which targets the C1 domain of FVIII and inhibits platelet surface binding as well as vWF binding. The crystals grown resulted in a structure with a resolution of 3.9 Å, r-free of 0.34 and r-work of 0.27. This structure is the first crystal structure to date showing complete FVIII bound to an inhibitory antibody fragment and sheds new light on the physiological function of FVIII with respect to its binding interactions. The second structure is of Et3i bound to Til'E', the domains of vWF which give rise to the high-affinity interaction with FVIII. This structure consists of two copies of FVIII at a resolution of 2.8 Å. Unfortunately, the model is not

complete and appears to not contain the Til'E' domains. However, the data is the highest resolution ever collected for FVIII and, when completed, the structure will allow for improved insight into the function of FVIII.

Acknowledgements

My path to a Masters degree has followed a tortuous path. My first educational adventures were at home. My mother educated me until I went to community college, so I have her and Saxon Math books to thank for learning how to read, write and put numbers together.

After blundering through general chemistry in community college I was grateful to receive an outstanding undergraduate education at Western Washington University. Of note, Dr. George Kriz taught my first organic chemistry class where I was both laughed at by the venerable professor for audibly proffering the incorrect interior angle for cyclopentane whilst simultaneously encouraged by academic success.

After a number of years which included making wine in two hemispheres, hunting orchids in Laos and sampling urine in Seattle, I came back to Western Washington University to obtain a masters degree in chemistry. Dr. Clint Spiegel graciously re-accepted me into his lab (I had spent some time there as an undergraduate dirtying dishes and eating sandwiches) and set me up on some projects which were likely impossible. The rest will be regarded as history in the future.

At this time I'd also like to thank my advisory committee, Dr. Jeanine Amacher and Dr. Spencer Anthony-Cahill as well as fellow Spiegel Lab members Ian Smith, Shaun Peters, Anne d'Aquino, Justin Walter, Michelle Wuerth, Connor Garrels, and Lexi Jarvis and all the others who helped me on my path.

Table of Contents

Page

Abstract.....	iv
Acknowledgements.....	v
List of Figures.....	vii
List of Tables.....	ix
List of Abbreviations.....	x
Introduction.....	1
Research Aims.....	17
Materials and Methods.....	18
Results.....	28
Discussion.....	41
Conclusion.....	53
Works Cited.....	54
Appendix.....	60

<u>List of Figures</u>	Page #
Figure 1. The coagulation pathway.....	2
Figure 2. Platelets.....	3
Figure 3. Two different visualizations of the blood coagulation cascade.....	5
Figure 4. FVIII domain organization.....	6
Figure 5. Structure and domain organization of B-domain deleted FVIII.....	6
Figure 6. A cryo-EM model for the interaction of D'D3 region of vWF with FVIII.....	7
Figure 7. Domain organization of vWF.....	8
Figure 8. Model of interaction between platelet surface and Factor VIII.....	10
Figure 9. Schematic model showing the principles of inhibitor formation.....	14
Figure 10. Workflow of structural determination by x-ray crystallography.....	26
Figure 11. Antibody purification analysis with 12.5% SDS-PAGE.....	28
Figure 12. C1 domain interaction with antibody 2A9 data from BLI experiment.....	29
Figure 13. Analysis by 12.5% SDS-PAGE of papain cleavage of antibody 2A9.....	30
Figure 14. Analysis of Til'E' construct protein purification by 12.5% SDS-PAGE.....	31
Figure 15. Analysis of cleaved Til'E' protein by 12.5% SDS-PAGE.....	31
Figure 16. Reproducible crystal morphology of 2A9:Et3i complex.....	33
Figure 17. Crystal of FVIII:Til'E' complex.....	33
Figure 18. Image of crystal mounted in loop in front of detector.....	34

Figure 19. Diffraction data images for 2A9:Et3i and Til'E':Et3i complexes.....	35
Figure 20. Molecular replacement solution strategy for 2A9:Et3i complex.....	37
Figure 21. FVIII chimera Et3i bound to FAb 2A9.....	37
Figure 22. Working model of FVIII:Til'E' complex with a notable absence of Til'E'.....	38
Figure 23. The interaction between FVIII and FAb 2A9 showing stick models.....	39
Figure 24. A hydrophobic interaction involving F2068 on the C1 domain of Et3i.....	39
Figure 25. C1 domain W2070 interacts with Y32 and N101 on the light chain of 2A9.....	40
Figure 26. Intimate contacts between C1 domain H2155 and residues on the heavy chain of 2A9.....	40
Figure 27. Interactions of T1744 of the A3 domain of FVIII and S92 of the heavy chain of 2A9.....	41
Figure 28. The site of interaction with the closest contacts is F2068 on the C1 domain of FVIII.....	42
Figure 29. Interactions with loop 2060-2070 on C1 domain.....	43
Figure 30. Antibody B136 epitope on C1 domain of FVIII.....	44
Figure 31. A lack of electron density.....	46
Figure 32. Model of Til'E' from PDB ID: 6N29.....	47
Figure 33. Cleavage of monoclonal antibody to make Fab.....	49

List of Tables

Page #

Table 1. Coagulation factors and associated proteins.....	3
Table 2. Affinity of Interaction Between FVIII and vWF.....	9
Table 3. Anti-C1 Antibody Interference in FVIII Function.....	18
Table 4. Biolayer-Interferometry Experimental Parameters.....	20
Table 5. Proteins in Buffers Prior to Complex Formation.....	23
Table 6. Crystallization Strategies Employed.....	24
Table 7. Cryo-protectants Used.....	25
Table 8. X-ray data collection parameters.....	26
Table 9. Pre-cleavage protein A+ purification results.....	29
Table 10. Lead crystallization conditions from Hauptman-Woodward crystal screen.....	32
Table 11. Processed diffraction data statistics for 2A9:FVIII complex.....	35
Table 12. Processed diffraction data statistics for Til'E':FVIII complex.....	36
Table 13. Statistics for current models of structural complexes.....	35
Table 14. Papain cleavage errors.....	51

List of Abbreviations

CDR Complementarity-determining region

ELISA enzyme-linked immunosorbent assay

FAb Fragment antigen binding

FIX Factor IX

FVIII Factor VIII

FVIIIa Activated Factor VIII

FIXa Activated Factor IX

IgG Immunoglobulin G

IMAC Immobilized metal affinity chromatography

kDa kilodalton

PC:PS phosphotidyl choline:phosphotidyl serine

PEG polyethylene glycol

PHENIX Python-based Hierarchical ENvironemnt for Integrated Xtallography

SDS-PAGE Sodium Dodecyl Sulfate Polyacrylamide Gel Electrophoresis

SEC Size exclusion chromatography

SHG Second harmonic generation

Spectra BR Ladder Spectra broad range ladder

vWF von Willebrand Factor

XDS X-ray diffraction software

Introduction

Homeostasis

The cardiovascular system is the organ responsible for providing tissues with oxygen and nutrients as well as carrying away waste products. It is the main transportation system of the body and comes into contact with every living cell. Maintenance of this system is of paramount importance due to the high oxygen and sugar requirements of cells. An acute drop in blood pressure due to injury results in near instantaneous loss of consciousness and concomitant brain-death.

An important consideration when thinking about vasculature is the fact that the bloodstream is essentially a leaky pipe. It would be ineffective if it either let out all of its contents out or was entirely impermeable. Fortunately, the body is able to produce an entire suite of proteins which both maintain an acceptable level of colloid osmotic pressure which holds fluid in the bloodstream as well as forming a built-in coagulation system which responds nearly instantaneously to any injury.

Coagulation

Coagulation is a broad term which means congealment or curdling: the formation of a solid out of a liquid¹. When an injury occurs to the bloodstream, a well-characterized biochemical pathway proceeds to re-establish homeostasis. First, endothelial cells which make up the lumen of blood vessels contract. Next, a platelet plug forms. The final step is formation of a hard clot. In blood there are soluble fibers called fibrinogen which ordinarily float along in solution. When these fibers are proteolytically cleaved, they are converted to insoluble fibrin. These insoluble fibrin molecules are covalently cross-linked in order to form the solid blood clot (figure 1).

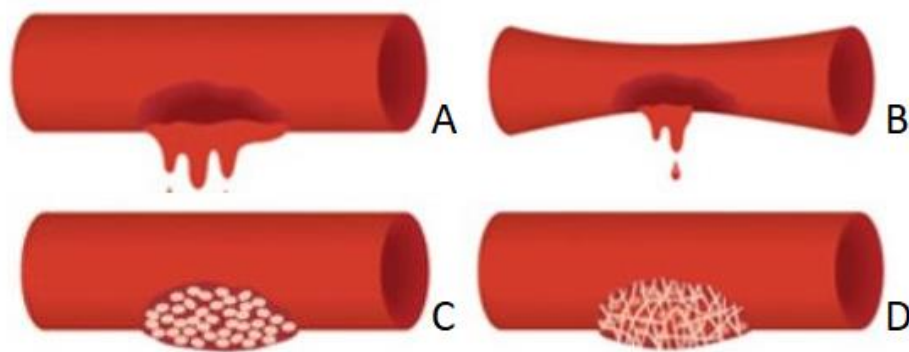


Figure 1. The coagulation pathway starts with an injury (A) followed by contraction of endothelial cells (B), platelet plug formation (C) and a cross-linked fibrin clot (D)³

An over-view of coagulation must start with an introduction of the primary actors. These are cells (platelets and endothelial cells), coagulation factors, and lipids (on cell surfaces).

Endothelial cells form the interior physical surface of blood vessels. These are elongated simple squamous cells which form the actual tube which blood flows through. Interior and exterior surfaces are different. Chemical signals such as histamine control the leakiness of a blood vessel at any given point in time. Upon injury, changes in cellular morphology controlled by cytoskeletal elements can open fenestrations which allow proteins and blood cells to interact with interstitial fluid.

Platelets, also called thrombocytes, are anucleate blood cells which are about one-tenth as large as red blood cells. They are produced in the bone marrow as megakaryocytes and are cytoplasmic fragments thereof. The ratio of platelets to red blood cells is approximately 1:10 in most healthy adults. When in normal circulation, platelets are discoid and approximately 2-3 μm across. Upon activation, they adopt a stellate morphology, secrete clotting factors such as vWF and fibrin, and, through specialized transmembrane proteins called flippases, present an anionic surface which notably has an approximately ten percent *o*-phosphatidyl serine composition.

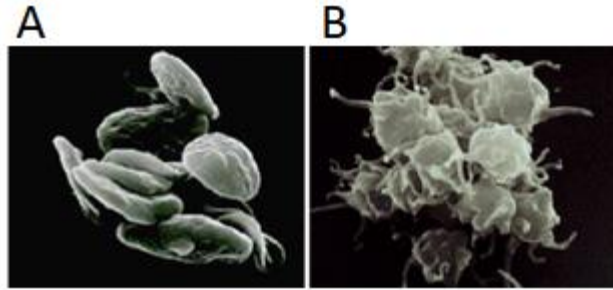


Figure 2. Platelets are normally round (A) but adopt a stellate morphology upon activation (B).

There are two primary routes which result in the blood coagulation cascade. These are referred to as the intrinsic and extrinsic pathways. The word cascade is used because there are a series of positive-feedback loops involving proteolytic activation. Coagulation factors are a suite of proteins which interact with each other in order to facilitate coagulation. The various factors involved are listed in Table 1 below.

Table 1. Coagulation factors and associated proteins

Coagulation Factors and Associated Proteins	Function
Factor I (fibrinogen)	Forms clot (fibrin)
Factor II (prothrombin)	Its active form (IIa/Thrombin) activates I, V, X, VII, VIII, XI, XIII, protein C, platelets
Factor III (tissue factor)	Co-factor of VIIa (formerly known as factor III)
Calcium (Factor IV)	Required for coagulation factors to bind to phospholipid (formerly known as factor IV)
Factor V	Co-factor of X with which it forms the prothrombinase complex
Factor VII	Activates IX, X
Factor VIII	Co-factor of IX with which it forms the tenase complex
Factor IX	Activates X: forms tenase complex with factor VIII
Factor X	Activates II: forms prothrombinase complex with factor V
Factor XI	Activates IX
Factor XII	Activates factor XI, VII and prekallikrein
Factor XIII	Crosslinks fibrin
von Willebrand factor	Binds to VIII, mediates platelet adhesion
Protein C	Inactivates Va and VIIIa
Protein S	Cofactor for activated protein C (APC, inactive when bound to C4b-binding protein)

The extrinsic pathway is so named because of its occurrence from the outside of the bloodstream. Upon tissue damage occurring, factor VII bind to tissue factor (a transmembrane protein in sub-endothelial cells) and is converted to factor VII activated. This complex activates Factor X to FXa. FXa activates thrombin and works in conjunction with the extrinsic pathway as described below. The FVIIa:TF complex has a high affinity for FIXa.

The intrinsic pathway occurs on the inside of the bloodstream. Upon blood vessel damage occurring, FXI is converted to FXIa in the presence of increased levels of calcium. FIX is activated by FXIa to FIXa. FVIII is converted to FVIIIa by thrombin. FIXa has a high affinity for FVIIIa which together bind on platelet surfaces form a “tenase” complex. This name comes from the fact that this complex results in the rapid activation of FX.

The pathways then work together; FXa binds to FVa which creates a complex that converts prothrombin (FII) to thrombin (FIIa). Thrombin, in turn, cleaves fibrinogen into fibrin, which forms long strands which are covalently bonded together to form blood clots by fibronectin and FXIII. This pathway is outlined schematically in figure 3.²

After a clot has been formed, it is necessary to stop the coagulation process. Protein C inactivates FVa and FVIIIa. This results in inactivation of FX as well and the cessation of fibrin generation.

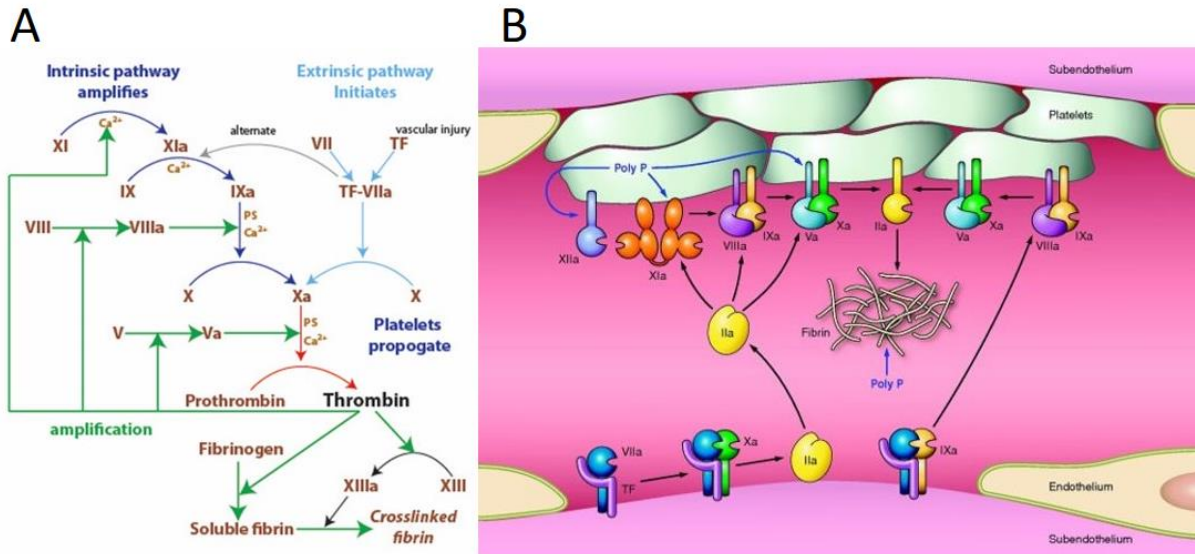


Figure 3. Two different visualizations of the blood coagulation cascade with the intrinsic and extrinsic pathways outlined schematically (A)⁴ and graphically (B)².

FVIII

FVIII is a large glyco-protein which is an essential part of the blood coagulation pathway. It is synthesized from a gene call *f8* on the X chromosome comprised of 186,000 base pairs. The FVIII gene is approximately 0.1% of the X chromosome and includes twenty-six exons ranging in size from 69-3106 bp and introns up to 32.4 kilobases. The actual coding mRNA is approximately 9000 base pairs long. Full length FVIII is 2332 amino acids in length and has a domain organization of A1-A2-B-A3-C1-C2.⁵

The A domains share 30% homology and the C domains share 37% homology. The intron locations reveal that most likely the multi-domain structure evolved due to duplication events within the gene.⁷

FVIII circulates as a heterodimer of A1-A2/A3-C1-C2 which are referred to as the heavy and light chain respectively. The actual structure of FVIII as solved by x-ray crystallography is shown in figure 3.⁶

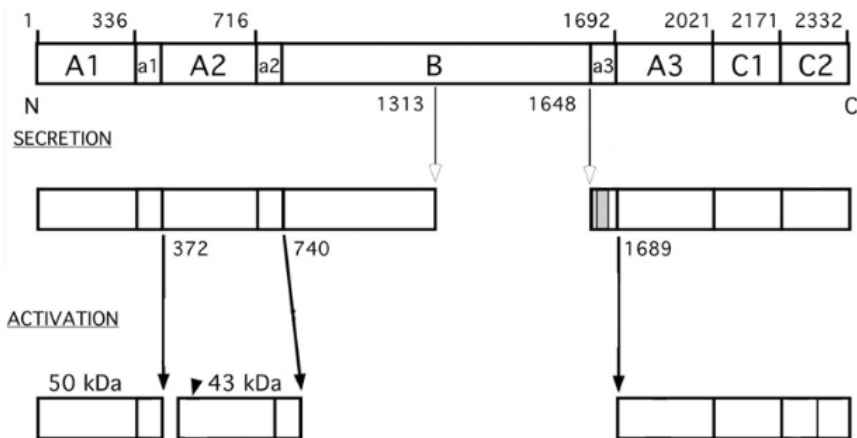


Figure 4. FVIII domain organization showing cleavage sites necessary for secretion and activation.⁶

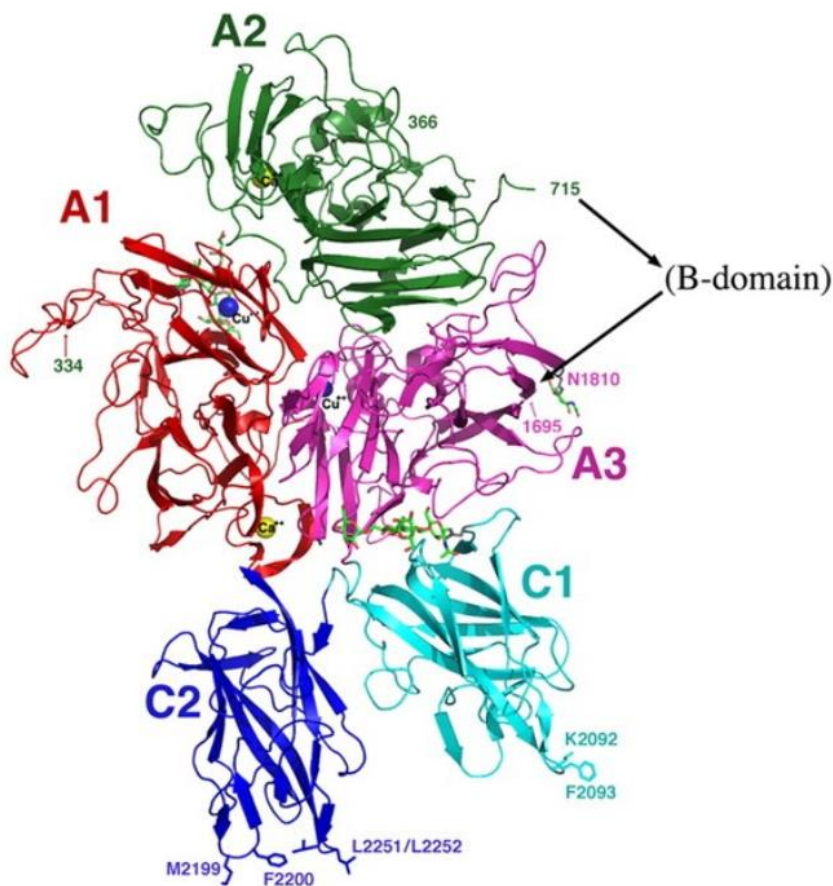


Figure 5. Structure and domain organization of B-domain deleted FVIII.⁶

Synthesis is thought to occur in endothelial cells. FVIII undergoes extensive posttranslational modification including sulfonation and glycosylation such as vitamin k dependent gamma glycosylation of glutamic acid residues.⁸

Interaction of FVIII with vWF

After synthesis and modification, FVIII is secreted and circulates bound to vWF. As a chaperone, vWF holds FVIII with 0.4 nM affinity.⁹ The current model of this interaction (figure 4) is through the D'D3 region of vWF and the light chain (A3-C1-C2) of FVIII. Specifically, a basic cleft along the backside of the C1 domain is complemented by sulfonated tyrosine (residue 1680) on a long loop on the A3 domain to bind the D' domain of vWF.

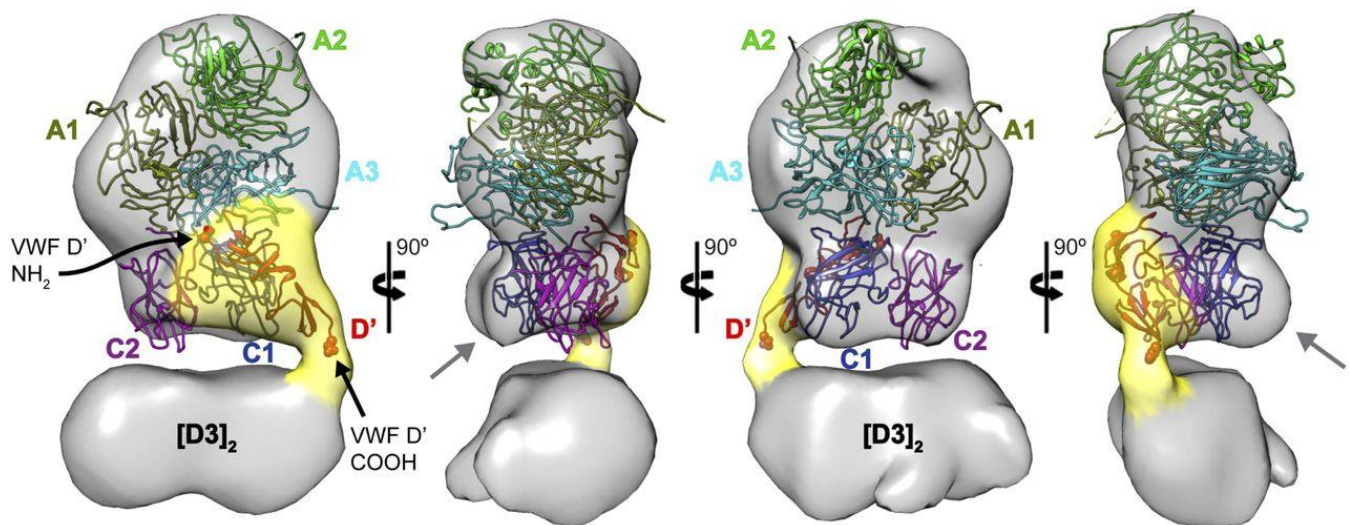


Figure 6. A cryo-EM model for the interaction of D'D3 region of vWF with FVIII.¹⁰

vWF is a large multi-domain glycoprotein which is 2813 amino acids long. After post-translational cleavage and modification, vWF forms multimers which can be megadaltons in mass. The D'D3 domains interact with FVIII. More specifically residues 763-864 comprise the Til'E' domains which provide the high-affinity site for FVIII binding by vWF.

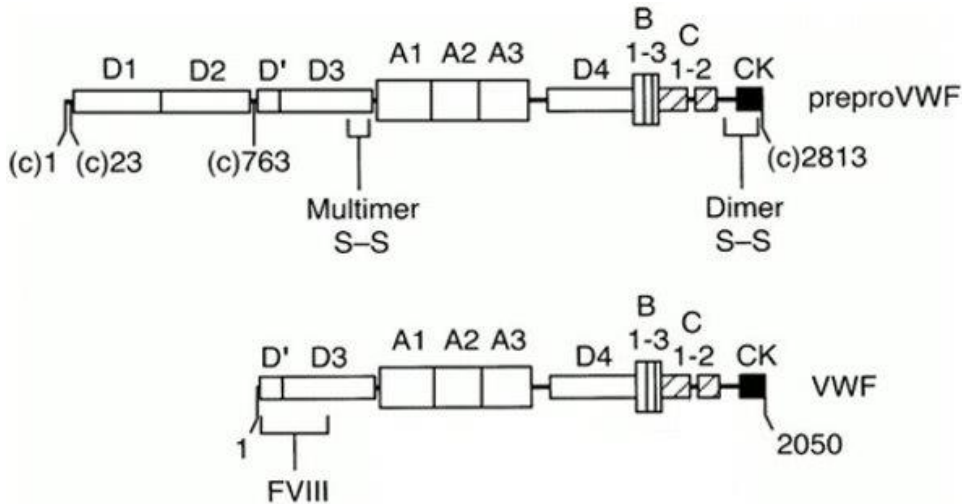


Figure 7. Domain organization of vWF showing the proenzyme and after cleavage.¹¹

Identification of the high-affinity site of FVIII interaction of vWF was achieved using a tryptic fragment of residues 767-1031. This fragment was found to strongly inhibit the binding of FVIII to vWF. Once this was discovered, it was mapped onto the sequence of vWF and the domain D', composed of Til' and E' was identified.¹²

A recent study determined that the entire D'D3 portion of FVIII is required for optimal binding. This is proposed to be because the D3 domain is able to reach under the C domains and stabilize interactions of the hydrophobic spikes. It was shown that D3 by itself did not bind effectively to FVIII, but mutations in the D3 region did significantly alter FVIII binding of the entire D'D3 construct.¹³

The exact nature of the interaction between FVIII and vWF has been studied by a variety of techniques. The affinity between Til'E' and FVIII varies widely between different studies. It has been shown through a mutation study of FVIII residue tyrosine 1680 to phenylalanine that the sulfonated tyrosine is essential for binding. This mutation entirely abrogated binding of FVIII to vWF.¹⁴

Table 2. Affinity of Interaction Between FVIII and vWF

Interaction	Method	Affinity (Kd)
Til'E':FVIII	Isothermal Titration Calorimetry ¹⁵	330 nM
Til'E':FVIII	Enzyme linked immunosorbent assay (ELISA) ¹⁶	26 nM
pdvWF:FVII I		0.9 nM
D'D3:FVIII	Biolayer-interferometry (BLI) ¹⁰	0.9 nM
VWF residues764- 1035:FVIII		3.8 nM

Physiological Function of FVIII

Upon vascular injury, vWF concatamers unwind and bind to receptors on endothelial cells and platelet surfaces near the site of injury. Specific residues on FVIII are then cleaved by thrombin to enable release from vWF and activation. Thrombin is a serine protease which cleaves in the acidic region of FVIII to create a heterotrimer of A1/A2/A3-C1-C2. Also cleaved is a forty amino-acid “latch” of residues 1648-1692 at the beginning of the A3 domain which is essential to the high affinity interaction between FVIII and vWF (figure 4).^{17,18}

After activation, free-floating FVIIIa must localize itself on the plasma membrane. This occurs through a specific interaction between the “feet” on the C domains of FVIIIa and *o*-phosphatidyl serine which is presented on the surface of activated platelets (figure 8). The key residues involved are hydrophobic spikes and key basic residues (arginine and lysine) which are spatially located to interact with *o*-phosphatidyl serine. There have been several attempts to show a “high-affinity” interaction site which determines the exact residue, but it seems that an avidity effect of having two C domains which each bind with multiple basic residues to the platelet surface is responsible for the strong binding interaction. The strength of the interaction has been determined to be 2 nM.^{19,20}

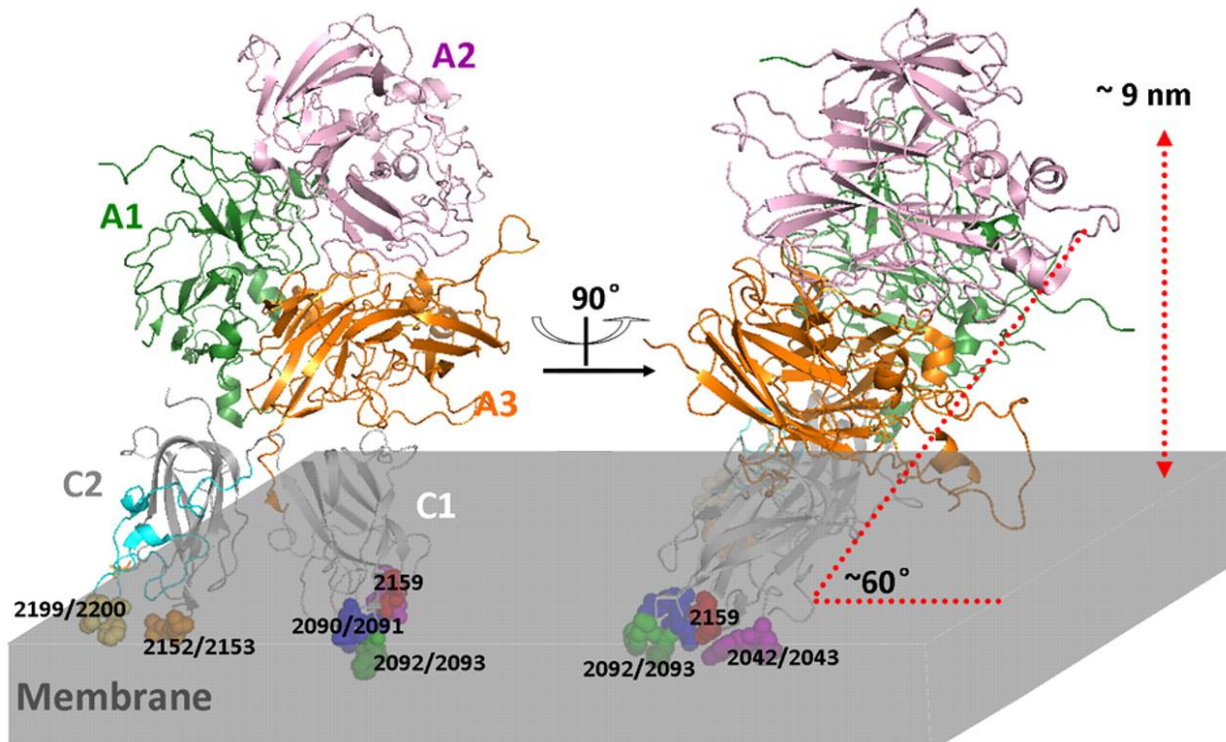


Figure 8. Model of interaction between platelet surface and Factor VIII (PDB ID: 3CDZ) with numbering of residues essential to binding interaction.¹⁹

To form the final “tenase” complex, FVIIIa binds FIXa. By locating FIXa on the activated platelet surface, FVIIIa increases the rate of fibrin clot formation 100,000 fold. The location of this interaction was first discovered by using sequential digest of FVIII which intefered with the binding of an antibody which in turn interfered with the FVIIIa:FIXa interaction. The exact region of binding is in the residue range 1778-1840 on the light chain and has an affinity of around 15 nM.²¹

FVIII Clearance

Because coagulation is the function of FVIII, it is important that the circulating level of FVIII is tightly regulated in order to prevent excessive bleeding or clotting. There is evidence that FVIII clearing is biphasic.

The putative fast clearance of FVIII is mediated by hepatic low-density lipoprotein receptors (LDLR) and LDLR-related protein (LRP). The binding interaction was localized to the A2 domain, specifically

residues 484-509. This leads to uptake of FVIII and degradation in the liver. This binding interaction was shown through solid-phase binding assays with ¹²⁵I-labeled FVIII full length, A1-A2 domains, A3-C1-C2 domains, and a peptide consisting of amino acids 484-509 of the A2 domain. These residues were chosen because it had been shown that an A2 targeting antibody previously had targeted these residues and inhibited binding of A2 to LRP.²² Later tests performed internalization assays with alanine mutants of FVIII and found that cellular uptake was decreased when the residues 484-509 were mutated.²³ The slow clearance of FVIII may be by the asialoglycoprotein receptor and is mediated by its glycosylation state. As FVIII circulates in the bloodstream, it is progressively “deglycosylated” enzymatically. This change results in increased affinity for receptors which result in the degradation of FVIII.²⁴ There is evidence that FVIII is taken up by macrophages when it is in complex with vWF. This was determined by radiolabeling vWF and staining mouse sections to determine location of protein. Co-localization with hepatic and splenic macrophages was observed.²⁵

Disorders in Coagulation

Due to the many factors involved in hemostasis, there are a wide range of diseases which affect different parts of the coagulation cascade.

Hemophilia is a disorder which affects the body's ability to maintain homeostasis by forming blood clots. There are several types of hemophilia based on which clotting factor is affected. Hemophilia A is due to decreased levels of FVIII. Hemophilia B is due to a deficiency of FIX. Less common hemophilias are hemophilia C which is due to a deficiency of Factor XI and parahemophilia which is due to a deficiency of Factor V. These hemophilias are all due to genetic mutations. In general, mutations can be classified as either null, truncation, or point. Null mutations result in a complete loss of expression. Truncation mutations result in a partial protein product being expressed. Point mutations result in

specific amino acid changes which can have significant effects on protein function. Some mutations cause an inversion of a specific exon in the transcript such that a functional protein is not produced.²⁶

As discussed above, the formation of the “Tenase” complex between FVIIIa, FIXa and the activated platelet surface is a crucial part of the blood coagulation pathway, increasing the rate of fibrin clot formation 100,000-fold. Based on the knowledge of this mechanism, it comes as no surprise that a deficiency of FVIII results in a problem with blood clotting.

Hemophilia A is an X-linked recessive disease which occurs in 1 in 5000 males. Point mutations have been documented in domains on FVIII which can affect the binding to vWF, activated platelet surfaces, FIXa, as well as increased degradation rate.

The severity of hemophilia A is described as mild, moderate or severe depending on FVIII function as >5%, 1-5% or <1% as determined by clotting assay. To assess FVIII function, the activated partial thromboplastin time is determined. The activated partial thromboplastin time assay measures the amount of time required for clotting.⁷

Another form of hemophilia which does not have a genetic basis is called acquired hemophilia A. This occurs when the body begins producing antibodies against FVIII which result in its rapid clearance and loss of function. The associated causes include cancer, lupus and pregnancy. A fuller discussion of inhibitor antibodies and their effects on FVIII will be included later in the introduction.

Von Willebrand's Disease (vWD) is when the *in vivo* chaperone of FVIII, vWF, has mutations which affect its function. Depending on the location of the mutation on vWF, there are three different types of vWD. Type 1 is a heterozygous mutation resulting in lower than normal expressed levels of vWF. Type 2 is characterized by mutations occurring in specific regions along vWF. Type 3 is a complete absence of vWF production and is the most severe form.

Type 2N vWD negatively impacts the ability of vWF to bind to FVIII. By looking at the point mutations which have resulted in this disease, much information concerning the exact interactions between vWF and FVIII has been elucidated. The binding region of vWF to FVIII has been isolated to the D'D3 region, and more specifically the 'Til'E' domains on vWF and the light chain on FVIII.

Hemophilia A Treatment

Treatment for hemophilia A consists of regular injections of FVIII into the bloodstream. Dosage frequency and amount depends on the severity of the disease. Costs of injections can add up to \$400,000 annually. There are currently many alternative drugs available when it comes to FVIII replacement therapy. This therapy works for many patients but the short half-life of FVIII, high cost, and antibody-inhibitor development in nearly a third of patients leaves much room for improvement in hemophilia A therapy.^{27,28}

Problems With Therapy: Inhibitor Development

The largest hurdle to effective FVIII replacement therapy is the formation of inhibitor antibodies which target FVIII. For nearly a third of hemophiliacs who receive FVIII injections, the immune system develops antibodies against an epitope on FVIII such that the body is essentially vaccinated against FVIII. There are numerous genetic and environmental factors which affect the risk of inhibitor formation. Before going into the specific risk factors which have been identified for FVIII inhibitor formation, I will first provide an overview of how antibodies develop.

When any molecule enters the bloodstream via injection, it is subjected to the scrutiny of the immune system as is any other chemical component already present. In general, small molecules such as amino acids, lipids and sugars are not able to illicit an immune response. Molecules which do illicit an immune response are called antigens. Antigens can range in size from oligopeptides to full proteins, as is the case

with FVIII, but can also include polysaccharides and small molecules which are joined to a larger molecule.

When a protein enters the bloodstream and is bound by a surface antigen-receptor on a B cell, the protein is endocytosed, degraded and its fragments are exposed bound to major histocompatibility II molecules. Helper T cells (CD4+) then stimulate the B cell to make specific antibodies against the exposed peptide fragment if they recognize the antigen fragment as a foreign agent.²⁹

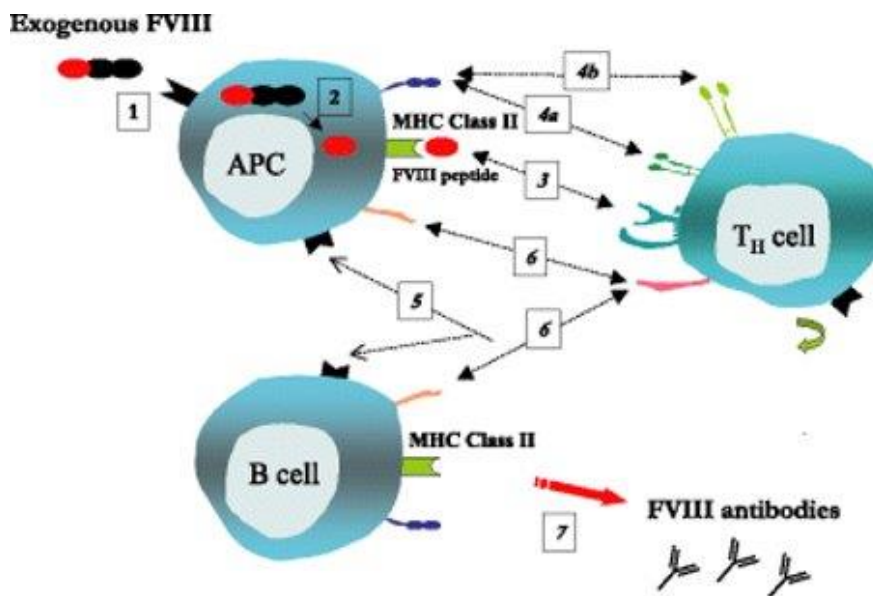


Figure 9. Schematic model showing the principles of inhibitor formation in patients with Hemophilia A (1. Injected FVIII binds to antigen-presenting cell and is endocytosed; 2. proteolytically cleaved peptides are presented; 3. Major histocompatibility class II molecules bind to peptide which is then presented to T-cells; 4a&b. co-stimulatory needed to stimulate cytokine release by T-cell; 5. Cytokine binding up-regulates immune activation in B- and T-cells; 6. B-cell proliferation, differentiation and antibody production is stimulated)³⁰

The B cell then produces clones which make more antibodies which specifically target the antigen. Most of the B cells die off but some remain as memory B cells which are activated to make clones which secrete more antibodies in the case of a future exposure to the antigen.

Stimulating immunogenicity is the goal of vaccination programs. However, when proteins are administered therapeutically, avoiding an activating immune response which results in memory B cells

is the goal. A major problem with protein therapeutics is that they are immunogenic. This is an issue with all therapeutic proteins including insulin and human growth hormone. The main factors which affect inhibitor formation against FVIII can be summarized as either genetic, environmental or treatment-related.^{31,32,33}

The major genetic factor is the type of mutation which leads to hemophilia A. Null mutations, which result in no FVIII protein being produced are the most likely to lead to inhibitor development. Point or small indel mutations where a FVIII protein is still produced are less likely to lead to inhibitor development. Only five percent of patients with minor mutations develop inhibitors.³⁴ This is thought to be because where there is no native FVIII antigen, there is no negative selection in the thymus to allow for tolerance of the injected FVIII. The other significant genetic factors are major histocompatibility (MHC) class and race. Significantly, patients from Caucasian backgrounds are half as likely to develop inhibitor antibodies as those of African background.³⁵

Environmental factors affecting FVIII inhibitor development are the patient's age at start of treatment, type of FVIII used, mode of administration used and immune system state.

There has been a long debate regarding whether plasma derived FVIII (pdFVIII) or recombinant FVIII (rFVIII) is more immunogenic. Some studies have suggested a nearly two-fold increase in risk from use of rFVIII versus pdFVIII. However, inconsistent methods for measuring inhibitors and considering other risk factors have diminished the impact of this finding. Regardless, glycosylation state, purity, aggregation and whether FVIII is pre-bound to its chaperone, vWF, are all important factors which affect inhibitor development.

The mode of injection makes a significant difference in inhibitor development. Prophylactic injections at regular intervals with smaller doses results in a better outcome than continuous injection (CI) systems.

Although CI is easier to manage, it is possible that consistent exposure to the antigen proves more antigenic than periodic injection. Mishandled samples leading to oxidation, aggregation or other impurities increases the risk of immunogenicity.³⁶

The immune system state changes depending on the health of a patient. Surgery, large bleeds, and infections are all relevant factors. It is thought that increased exposure of the bloodstream to tissues increases immunogenicity. This idea is supported by inhibitor formation in previously healthy individuals following surgery.³⁰

Inhibitor Interactions with FVIII

Inhibitors can be classified based on whether or not they interfere with the physiological function of FVIII. These two types are called neutralizing and non-neutralizing antibodies, respectively.

Discovering if injected FVIII is functioning in a patient is determined by a Bethesda assay. Plasma from a hemophilia A patient is subjected to a series of dilutions, FVIII is added, and coagulation times are determined. The result is expressed in Bethesda units. A Bethesda unit (BU) is defined as the amount of inhibitor, which destroys one half of the FVIII activity in one ml of normal plasma within two hours when incubated at 37°C.³⁷ A high responding inhibitor is defined as having greater than five Bethesda units.

As the exact mechanism of function of FVIII has become nearly fully elucidated, it is clear that the location of the inhibitor is more important than the amount of inhibitor present. Neutralizing antibodies which abrogate FVIII function bind in locations to sterically interfere with platelet surface interactions, vWF binding sites or the FIXa binding site. Therefore, it is of significant interest in the ongoing treatment of hemophilia A to derive more structural data of FVIII interactions with both inhibitors and vWF.

Research Aims

To provide more information regarding the interaction of FVIII with vWF and inhibitor antibodies in order to improve therapies for hemophilia A, the following aims were put forward:

1. Co-crystallize FVIII variant Et3i with antigen binding fragments and solve the three-dimensional structure in order to better understand how inhibitor antibodies interfere with FVIII function.
2. Co-crystallize FVIII variant Et3i with the T1'E' domains of vWF and solve the three-dimensional structure in order to elucidate the exact interaction between FVIII and vWF.

Materials and Methods

Growth of Antibodies

Collaborators from the Lollar lab at Emory university gave us three different hybridoma cell lines which were engineered to express 2A9, B136 and M6143, murine monoclonal antibodies which target the C1 domain of FVIII. Antibody 2A9 was successfully crystallized and will be discussed throughout the rest of the paper.

Antibodies against FVIII were generated by injecting human FVIII into hemophilia A model mice, harvesting the spleen, and creating hybridomas which expressed monoclonal antibodies. The effects of the isolated antibodies on FVIII function were analyzed in terms of interference with vWF and platelet binding.³⁸

Table 3. Anti-C1 antibody interference in FVIII function.³⁹

Antibody	VWF binding IC50 (μg/mL)	Phospholipid binding IC50 (μg/mL)	Bethesda Units/mg IgG	Affinity (nM)
2A9	1.1	0.9	23	0.9 ± 0.2
B136	0.4	0.04	700	0.1 ± 0.03
M6143	0.6	>10	180	0.2 ± 0.1

Cells were removed from –80° C freezer and thawed rapidly at 37° C in a water bath then centrifuged at 6000 RPM for two minutes. The cell pellet was reconstituted in 2 mL of growth media (Stem Cell Technologies Clonacell HY Medium E – Cat # 03805) and placed into T-75 growth flasks in a 37° C incubator with 5% carbon dioxide gas atmosphere. Growth convergence on surface of flask and morphology were monitored. Growth media was added periodically to a total volume of 50 ml over the course of approximately one week. Once growth achieved ninety percent confluence, growth media was harvested and cells were pelleted at 6000 RPM for two minutes. The flask containing adhered cells was rinsed three times with three milliliters of phosphate buffered saline. Fifty milliliters of expression

media (CD Hybridoma Medium, Invitrogen # 11279 per 1000 ml of CD hybridoma media add 30 ml of GlutaMax-1, Invitrogen # 35050, 5 ml of 100x Penicillin/Streptomycin Invitrogen # 15140, and 4 ml of 250x Cholesterol Invitrogen cat # 12531) were then added to the washed, adhered cells and cells were allowed to express for a week. The pelleted cells from the growth media were transferred to a new T-75 flask and grown to confluence as outlined above. The cells were grown and expressed for four cycles before discarding.

After allowing cells to express, the expression media was harvested and centrifuged at 6000 RPM for 10 minutes to pellet out the cells. The supernatant was either placed at 4° C if the antibodies were to be purified soon or frozen by placing in negative -80° C for future use.

Purification of Antibodies

Hybridoma expression supernatant, thawed in fridge overnight if frozen, was diluted five times with nanopure water and pH was reduced to 6.0 by adding 0.5 M MES (pH unadjusted). The diluted, pH adjusted media was loaded at approximately 2 ml per minute onto a column containing SP Sepharose Fast Flow resin pre-equilibrated in binding buffer (10 mM MES; 200 mM NaCl; pH 6.0) as shown in figure 10. After loading, the column was washed with binding buffer until a baseline OD280 was achieved. Antibody bound to the resin was eluted using elution buffer (20 mM HEPES, 150 mM NaCl, pH 7.4). Elution fractions were concentrated using Amicon Ultra spin concentrator with a 30k molecular weight cut-off filter at 3500 g. Nearly all antibody elutes in first 3 ml elution fraction.

Purified antibody was analyzed using A₂₈₀ absorbance and SDS-PAGE. If product was non-homogenous, a protein A+ purification step was used to increase purity. A 0.2 ml protein A+ column was used. Antibody was incubated for ten minutes with end-over-end mixing in protein A+ column which had been pre-equilibrated in buffer (150 mM NaCl; 50 mM Hepes pH 7.4), washed three times

with buffer and then eluted with low pH buffer (0.1 M Sodium Acetate pH 3). Elution buffer was neutralized with a high molar strength buffer (1 M Tris pH 7.5). The sample was then reanalyzed for purity and flash frozen in liquid nitrogen for future use.

Biolayer-Interferometry (BLI)

In order to show binding between IgG 2A9 and the C1 domain of FVIII, BLI was employed. Ni-NTA tips were hydrated in buffer (50 mM Hepes pH 7.4; 150 mM NaCl) for ten minutes before being loaded onto BioForte Blitz instrument. The experiment consisted of baseline, association of HIS-tagged C1 domain construct previously purified in lab, followed by baseline, association of antibody, and dissociation steps. Shaking at 2000 RPM was utilized, and samples were spun down at 10,000 g for 5 minutes prior to experiment. C1 domain was loaded in a 4 μ l drop at a concentration of 40 μ g/ml. Association steps of antibody and control protein were performed in a 4 μ l drop at approximately 10 μ M. Baseline and dissociation steps were in a tube containing 250 μ l of buffer.

Table 4. Biolayer-Interferometry experimental parameters.

Experimental Step	Time (seconds)
Baseline	30
Load	60
Baseline	60
Association	120
Dissociation	120

Papain Cleavage of Antibodies

Purified antibodies were thawed on ice and dialyzed in papain cleavage sample buffer (10 mM EDTA; 20 mM sodium phosphate pH 7) before being concentrated in an Amicon centrifuge spin filter with a 30 kDa molecular-weight cutoff. Agarose-linked papain was equilibrated in digestion buffer (sample buffer + 30 mM cysteine and pH readjusted to 7) and combined with dialyzed antibody mixed 1:1 with digestion buffer in a 1.5 mL Eppendorf tube. The cleavage reaction was taped horizontally in benchtop

shaker at 37° C overnight shaking at 250 RPM to ensure continual mixing of agarose-linked Papain (ThermoScientific product # 20341). The crude cleavage product was harvested by filtering out agarose linked papain with a costar spin filter and washing agarose two times with 100 µl of neutralization buffer (50 mM Tris-HCl pH 7.4). The neutralization buffer washes were combined with crude cleavage supernatant and FAbs were separated from Fc regions with protein A+ purification as explained in the section above. In this case, however, the initial flow-through and first wash step contained pure FAbs. The cleavage product was then analyzed for purity by measuring the A₂₈₀, A₂₆₀ and SDS-PAGE. The pure product was flash frozen in liquid nitrogen for future use.

Growth and Purification of Til'E' Domains of vWF

The Til'E' domains of vWF, comprising residues 766-864, had previously been cloned into a pET32b1 vector containing an N-terminal thioredoxin (TRX) and HIS6 affinity tag. Cell stock of previously transformed cells containing the plasmid were thawed on ice. Growths of 2 µl cells in 50 ml of LB broth (for 1 L of LB broth: 10 g Bactotryptone; 5 g yeast extract; 10 g NaCl) and Ampicillin added to a concentration of 0.05 mg/ml were shaken at 180 RPM overnight at 37° C. Overnight growths were added to 1 L of LB broth with Ampicillin added to a concentration of 0.05 mg/ml. Cell growth was monitored by checking OD₆₀₀ until absorbance reached 0.6. At this point, IPTG was added to 1 mM and temperature was reduced to 15° C. Cells induced to express Til'E' overnight before being harvested by centrifugation at 6000 RPM for 10 minutes. The supernatant was discarded and cell pellet was resuspended in lysis buffer (500 mM NaCl; 20 mM Tris-HCL pH 7.5) with lysozyme at 1 mg/ml and PMSF at 1 mM and mixed for 30 minutes at 10° C. Three liters of growth per 30 ml of lysis buffer were used. Sonication was used to lyse cells at duty cycle 50, output 5 (Branson, Sonicator) two times for 45 seconds with a 30 second rest between rounds of sonication to prevent overheating of cells. Lysed cells were centrifuged at 17000 g for 45 minutes to pellet cellular debris. Supernatant was filtered

sequentially with 5 μ m and 0.4 μ m disposable syringe filters. Filtered supernatant was purified using IMAC with Talon resin (see appendix for more information). After elution with high imidazole buffer (500 mM NaCl; 20 mM Tris pH 7.5; 200 mM imidazole), protein was dialyzed into storage buffer (20 mM Tris-HCL pH 7.5; 100 mM NaCl; 2.5% glycerol) analyzed by SDS-PAGE and A₂₈₀ reading.

TEV Cleavage of Til'E' Construct

Purified Til'E'-Thioredoxin-HIS6 protein was thawed and cleaved with Tobacco Etch Virus (TEV) protein previously produced in the lab. TEV is a 27 kDa protease which cleaves the linear epitope EXXYXQ(G/S) where X can be any amino acid other than N. Cleavage occurs between Q and G. In this construct, the cleavage site was: ENLYFQ↓G. Cleavage took place by mixing TEV with the Til'E' construct at an OD₂₈₀ ratio of 1:10 (TEV:Til'E') and incubating at room temperature for three hours before transferring to 4° C fridge overnight. The cleaved Til'E' was separated from TEV and Thioredoxin-HIS6 by IMAC purification. Cleavage product was further purified using SEC as described in the next section. The final product was analyzed for purity and concentration by SDS-PAGE and A₂₈₀ reading.¹⁶

Size Exclusion Chromatography

Due to impurities present with Til'E' after expression and cleavage, SEC was utilized to further purify the protein. A Superdex 75 300/10 GL High Performance Column (product: 17-5174-01 GE life sciences) was pre-equilibrated with buffer (50 mM Tris HCl pH 7.4; 150 mM NaCl) and protein was loaded onto the column at a flow rate of 0.5 ml per minute using a 0.5 ml loading loop. The pressure limit was set at 1 MPa. Elution peaks were monitored which had a high UV reading and assessed for yield and purity by A₂₈₀ and SDS-PAGE.

FVIII Chimera ET3i

Et3i is a chimeric construct of porcine and human FVIII domains which is being developed as an alternative FVIII replacement therapy option by *Expression Therapeutics*. The B-domain is deleted, domains A1 and A3 are porcine, and domains A2, C1 and C2 are human. The main advantage of these changes are higher expression levels and an extended half-life. It was received at 0.84 mg/ml (5.6 uM) in storage buffer (350 mM NaCl; 50 mM Hepes pH 7.4; 5 mM CaCl₂).⁴⁰

Crystal Complex Formation

Complex of Et3i and 2A9 was formed by mixing proteins in Eppendorf tube on ice and allowing to sit for ten minutes. In order to ensure that all Et3i molecules were bound to antibody, a 1.2:1 molar ratio of antibody to Et3i was used.

Complex of Et3i and Til'E' was formed by mixing proteins in Eppendorf tube on ice and allowing to sit for ten minutes. In order to ensure that all Et3i molecules were bound to antibody, a 1.2:1 molar ratio of antibody to Et3i was used. In order to reduce the salt concentration to physiological concentration, the Et3i:Til'E' complex was diluted with a low salt buffer (Tris-HCl pH 7.4; 5 mM CaCl₂; 50 mM NaCl) and concentrated to achieve a final NaCl concentration of 150 mM. After making the complexes, aliquots of fifty microliters were flash frozen and placed at -80° C for future use.

Table 5. Proteins in Buffers Prior to Complex Formation

Protein	Concentration	Buffer
Et3i	5.6 uM	20 mM Hepes pH 7.4; 350 mM NaCl; 5 mM CaCl ₂
2A9 FAb	64 uM	50 mM Tris HCl pH 7.4; 150 mM NaCl
Til'E'	150 uM	50 mM Tris HCl pH 7.4; 150 mM NaCl

Hauptman-Woodward Crystallization Screen

An outside lab was contracted to search for leads in a crystallization screen which required 500 µl of sample to test 1536 unique conditions. The samples were prepared as described in the previous section, flash frozen in liquid nitrogen, and shipped to the Hauptman-Woodward Crystallization screening lab.

Crystallization Optimization

After analyzing image data from the Hauptman-Woodward crystallization screening service, a series of optimizations were performed which approximated the lead conditions discovered in the crystallization screen.

Hanging drop vapor diffusion was employed using a twenty-four well tray. In general, precipitant concentration was adjusted on one axis while pH was varied on the other. Crystallization strategies which were employed are outlined in table 6. The hanging drop was mixed on a glass cover slip with the mother liquor and sealed into the well using lubricant. A drop ratio of 1 µl protein to 1 µl mother liquor was used for the Et3i:2A9 complex while a 2:1 ratio was used for the Et3i:Til'E' complex.

Table 6. Crystallization Strategies Employed

Strategy Used	Notes
Making Full Set of Conditions	24 tubes were prepared individually
“4 Corners”	Four tubes were prepared, one for each corner of the tray, and mixed together to create a gradient in variables employed
Univariable	Two tubes were prepared and mixed together to create a one-variable gradient
Dope Salt	Wells were filled with 90% volume condition at 111% concentration and salt at 1 M concentration was doped in to achieve 0.1 M concentration salt

Completed trays were placed on foam at room temperature and checked frequently for crystal growth. When a crystallizing condition was discovered, another tray was prepared which focused more closely on the crystallizing condition.

Looping and Cryoprotecting Crystals

Crystals of notable size and appearance were captured for x-ray diffraction data collection. Two different strategies were employed for looping crystals. In one instance, crystals were transferred into a cryoprotectant solution and after five minutes of equilibration were looped with cryo-loops. In the other instance, cryo-protectant solution was added directly to the drop containing the crystal for equilibration prior to looping. Looped crystals were flash frozen and placed in a liquid nitrogen dewar for future collection of diffraction data.

Table 7. Cryo-protectants used contained matching drop buffer and components listed below.

Complex	Cryoprotectant utilized
ET3i:2A9	30% Glycerol
ET3i:2A9	30% PEG 400
ET3i:2A9	30% 1,4-propane-diol
ET3i:Til'E'	20%/30%/40% Glycerol
ET3i:Til'E'	20%/40% PEG 400
ET3i:Til'E'	30% DMSO

Overview of X-Ray Crystallography

The gold-standard for macromolecular structural determination is x-ray crystallography. The macromolecule of interest is crystallized and placed in front of a source of x-ray beams. The resulting diffraction pattern which is produced is composed of spots, each of which is due to a “structure factor” of electron density in the crystal. By taking a series of diffraction images each with the crystal rotated at a different angle, the pattern of spots can be merged together into a single dataset which calculates the amplitudes of electron intensity and unit cell size of the crystal. The mathematical operation which makes this possible is called the Fourier transform which, in general, is able to convert between frequency and time domains. This information is then converted to an actual 3D map of electron density when the phase of the diffracted x-rays is solved through molecular replacement. In this method, a

structure which is similar to the macromolecule of interest is superimposed on the map and electron density is assigned the correct phase. At this point, the final solution of the structure is determined by building in the sequence of the protein into the electron density map.

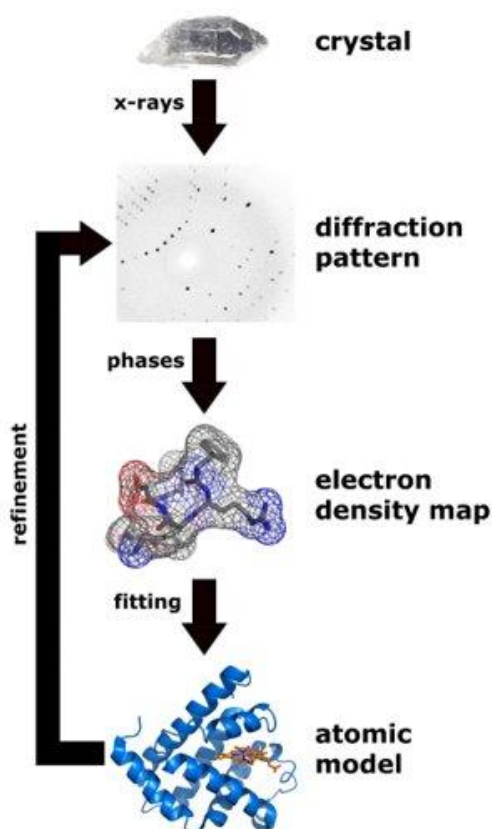


Figure 10. Workflow of structural determination by x-ray crystallography

Collection and Processing of Data

Cryoprotected crystals were shipped to the advanced light source (ALS) in Berkeley, California. X-ray diffraction data was collected remotely and analyzed using x-ray diffraction software (XDS).

Table 8. X-ray data collection parameters from XDS program

Parameter	2A9:Et3i	Til'E':Et3i
Detector Distance (mm)	600.00	500.00
X-Ray Wavelength (Å)	1.00000	0.97741
Oscillation Range (Degrees)	0.5	0.25
Images Collected	165	1440
X-Ray Source	Advanced Light Source Synchrotron, Berkeley, California	

Sequencing of 2A9 Antibody Heavy Chain and Light Chain

Upon successful solution of the 2A9:Et3i crystal structure, the 2A9 variable region sequence was determined by PCR at an external lab. The amino acid sequence for the variable and complementarity determining regions of the heavy and light chains were determined. Further information is included in the appendix.

Results

Antibody Purification

Harvested expression media containing antibody 2A9 was harvested and the antibody was purified as outlined in the methods section. A 12.5% SDS-PAGE analysis was performed with reducing and denaturing conditions and the eluted antibody can be seen in figure 12 as a heavy chain at 50 kDa and a light chain at 25 kDa.

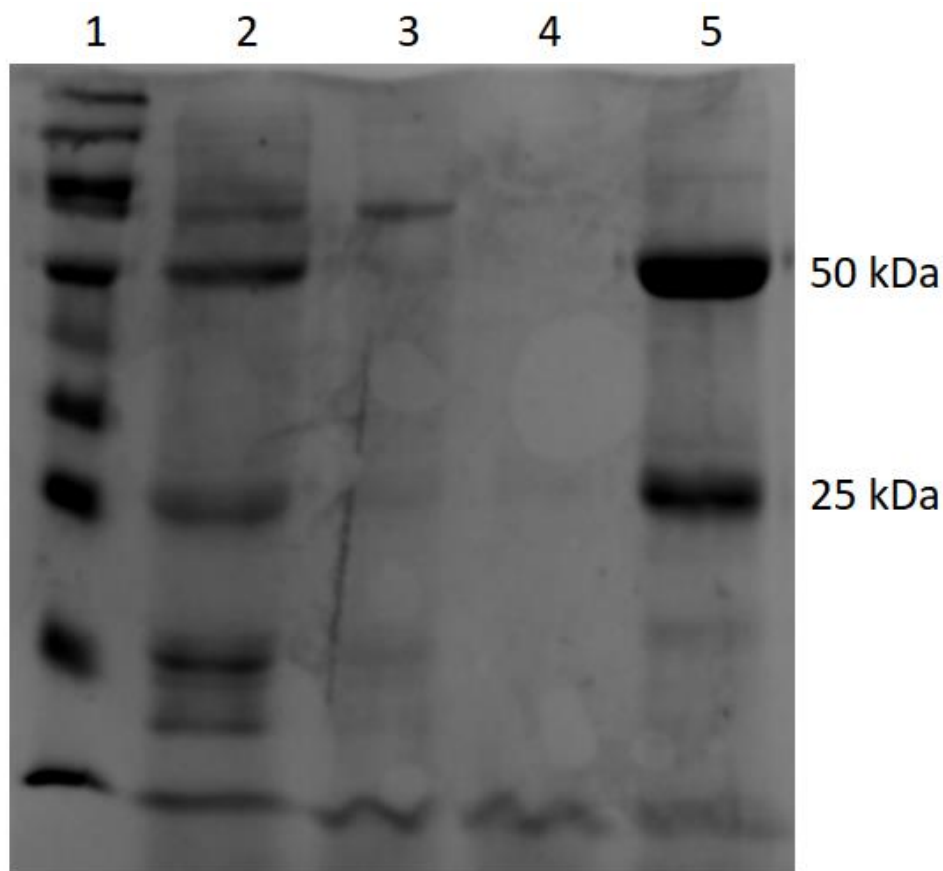


Figure 11. Antibody purification analysis with 12.5% SDS-PAGE gel of antibody 2A9 ion-exchange chromatography purification from August 30th 2018 (lane assignments left to right: 1. Spectra BR Ladder (10-150 kd) 2. Expression media supernatant 3. Concentrated flowthrough 4. Flowthrough non-concentrated 5. Elution)

In order to further purify the 2A9 antibody before cleavage, a protein A+ purification was performed on the elution from figure 12 (lane 5), the results of which are shown in table 9. The overall yield for this purification was only 1.5 mg of pure IgG.

Table 9. Pre-cleavage protein A+ purification results

	A ₂₈₀	Ratio (A ₂₆₀ /A ₂₈₀)	mg/ml	Volume (ul)
Flowthrough	5	1	3.7	400
Wash I	0.3	0.72	0.21	400
Wash II	0.1	0.6	0.08	400
Elution I	3.2	0.51	2.4	440
Elution II	1.3	0.515	0.85	440
Elution III	0.25	0.53	0.17	440

Biolayer Interferometry Interaction of IgG 2A9 with C1 Domain of FVIII

A BLI experiment performed clearly showed specific interaction of IgG 2A9 with the C1 domain of FVIII whereas a control protein did not interact at all. This technique was used as a qualitative test of binding and kinetic data was not collected. In biolayer interferometry, a signal which increases is due to more mass being attached to the sensor tip. Thus, an increase in signal can be inferred as a binding interaction. If signal does not decrease during the dissociation phase, the interaction is tightly bound and has a low off-rate. As seen in figure 13, the IgG 2A9 binds and creates a strong signal whereas the control protein does not.

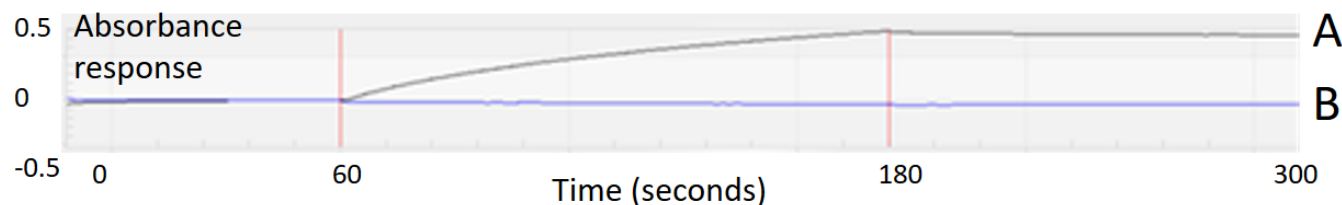


Figure 12. C1 domain interaction with antibody 2A9 data from BLI experiment showing control protein (A) and 2A9 (B) for a baseline step after C1 domain was loaded from 0-60 s, association of protein from 60-180 s and dissociation of protein from 180-300 s.

Papain Cleavage

Two lots of papain cleavage (A and B) were performed at a microscale. A 12.5% SDS-PAGE analysis was performed with reducing and denaturing conditions and the cleaved FAb can be seen in figure 14 as a band at 25 kDa. Note that the Fc region, which appears at around 35 kDa, only leaves the column when it is eluted. Lanes 1-5 were combined as purified FAb for crystallization studies. Lanes 7 and 8 show that the cleavage reaction did not go to completion and there is excess uncleaved IgG remaining. Lane 6 is not relevant.

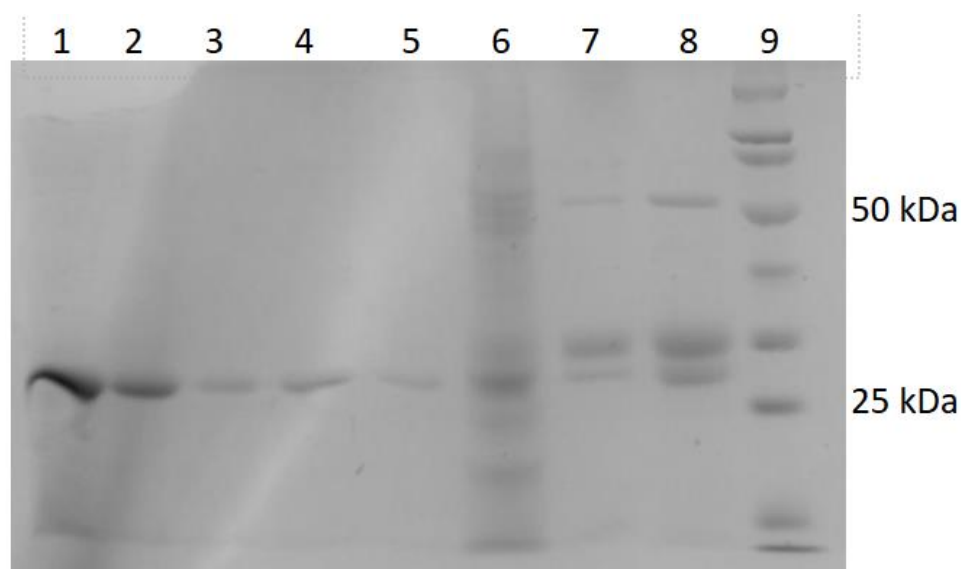


Figure 13. Analysis by 12.5% SDS-PAGE of two different papain cleavage lots of antibody 2A9 (gel layout 1. A Flowthrough 2. A Wash I 3. A Wash II 4. B Wash I 5. B Wash II 6. Pre-purification antibody 7. A Elution I 8. B Elution I 9. Spectra BR Ladder).

Til'E' Purification

The purification process of Til'E' was analyzed by 12.5% SDS-PAGE. Results from figure 15 A revealed that the initial product had contaminating bands throughout. The protein did express well. The elution fractions were further purified using SEC and the purified Til'E' construct can be seen in figure 15 B lane four.

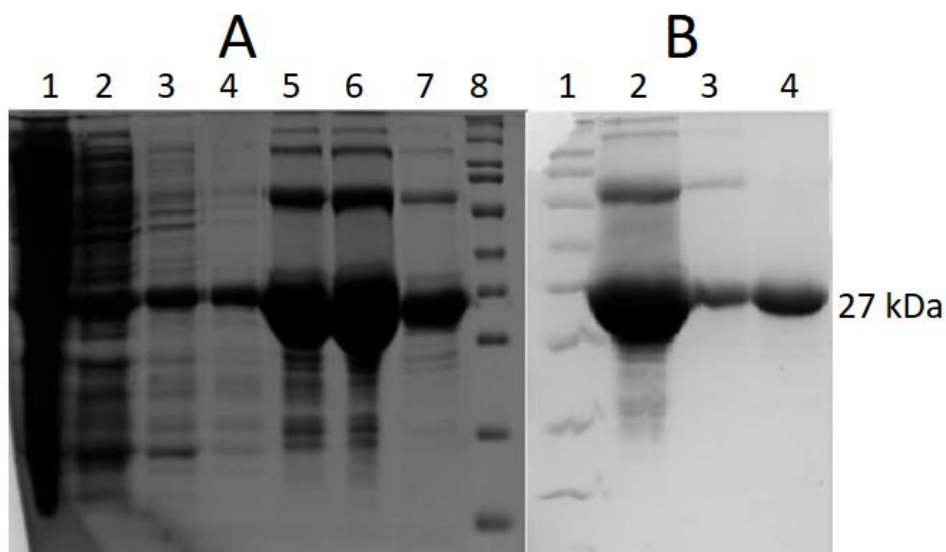


Figure 14. Analysis of Til'E' construct protein purification by 12.5% SDS-PAGE showing post IMAC Til'E' construct (A) and post SEC Til'E' construct (B). (Gel A layout: 1. Flowthrough. 2. Wash I. 3. Wash II. 4. Wash III. 5. Elution I. 6. Elution II. 7. Elution III. 8. Spectra BR Ladder. Gel B layout: 1. Spectra BR ladder. 2. Pre-SEC. 3. peak I. 4. Peak II.

Because the goal was to crystallize FVIII with just the Til'E' domain, TEV cleavage was performed on the linker region between the E' and thioredoxin domains. The result of the initial cleavage is seen in figure 16 A lanes two and three. In order to clean up the cleavage product, SEC was used and resulted in the final purified product seen in figure 16 B lane 2.

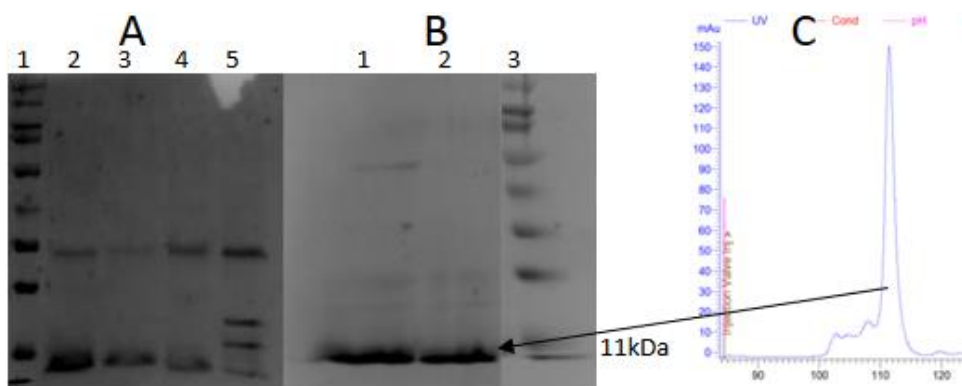
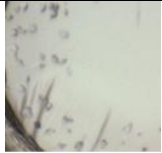
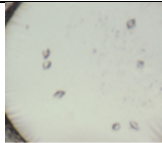
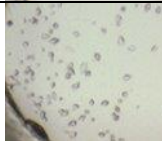

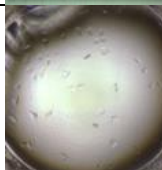



Figure 15. Analysis of cleaved Til'E' protein by 12.5% SDS-PAGE showing Post cleavage Til'E' (A), SEC purified cleavage product (B) and a chromatogram of the SEC purification of the cleavage product from gel A lane 2(C) (lane assignments: 1. Ladder; 2. Flowthrough; 3. Wash I; 4. Wash II; 5. Elution (b) 1. Pre-SEC pooled sample 2. Purest peak 3. Spectra BR ladder).

Hauptman-Woodward Crystallization Screen Results

A 1536 condition high-throughput screen by the Hauptman-Woodward lab of the complexes was analyzed by looking at photographs every week for six weeks. At week four, an SHG and UV image were also taken. Promising crystallizing conditions and images of the associated crystal are shown below in table 10 for the Et3i:2A9 complex and the Et3i:Til'E' complex.⁴¹

Table 10. Lead crystallization conditions from Hauptman-Woodward crystal screen

Complex	Condition #	Chemical Makeup	Image
Et3i:2A9	1030	8% (v/v) Tacsimate pH: 8, PEG 3350 20%,	
Et3i:2A9	1218	0.1 M Ammonium Tartrate Dibasic pH 7; PEG 3350 12%	
Et3i:2A9	1436	0.1 M Magnesium Formate Dihydrate; PEG 3350 15%	
Et3i:Til'E'	623	0.1 M NH4Br; 0.1 M Bis-Tris Propane pH 7; PEG 20000 12%	
Et3i:Til'E'	963	0.1 M LiBr, 0.1 M Bis-Tris Propane pH 7, peg 20000 12%	
Et3i:Til'E'	115	0.1 M Sodium Molybdate Dihydrate; 0.1 M Bis-Tris Propane pH 7; PEG 20000 12%	

Crystal Growth and Morphology

Crystals of the 2A9:Et3i complex were grown in conditions surrounding the PEG 3350 12-20%, pH 7-8 hits as shown above. When making the last column of conditions, the available stock of PEG 3350 was used up so the final column was switched to PEG 1500. Surprisingly, this resulted in crystal formation.

Further optimizations around the condition which worked arrived at a reproducible crystal morphology as shown in figure 17 below. The optimal condition was PEG 1500 17.5% and HEPES pH 7.7 with a 1 μ l protein to 1 μ l mother liquor drop size and ratio.

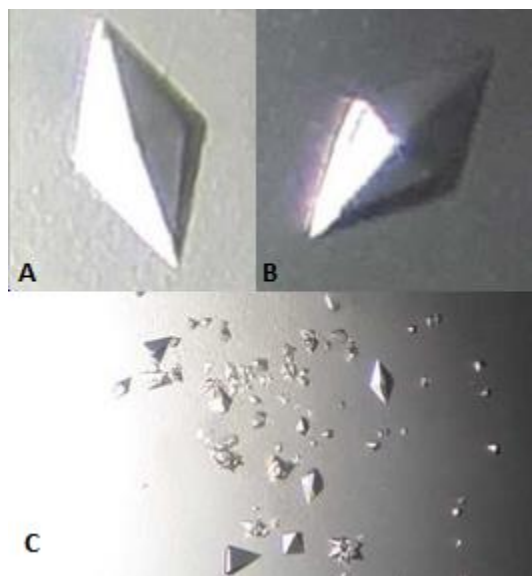


Figure 16. Reproducible crystal morphology of 2A9:Et3i complex photographed through microscope of a close-up of large crystals (A & B) and microcrystals (C).

Crystals of the FVIII:Til'E' complex were grown around the lead condition of 100 mM bis-tris propane pH 7 with PEG 20k 12% and salt. Six different salt dopes were used, and it was discovered that magnesium-nitrate resulted in large crystals being grown. After several round of optimization, the condition of 50 mM bis-tris propane pH 7, 14% PEG 20k, 200 mM magnesium-nitrate with a 2:1 ratio of protein to mother liquor in drop resulted in the crystals shown in figure 18.



Figure 17. Crystal of the alleged FVIII:Til'E' complex

Crystals were cryoprotected prior to being looped and flash frozen as described in the materials and methods section. The data sets were collected on cryoprotected crystals of 2A9:Et3i with 30% PEG 400 and Til'E':Et3i with glycerol 30%.

X-Ray Diffraction Data and Collection

Crystals which had been prepared for data collection were sent to the Advanced Light Source synchrotron in Berkeley, California in a liquid nitrogen shipping dewar. Remote data collection was performed from the Stoddard Lab at Fred Hutchinson Cancer Research Center in Seattle. A looped crystal is shown mounted on the goniometer head of the x-ray diffractometer in figure 19. Images of the actual diffraction patterns from which the crystal structures were solved are shown in figure 20.

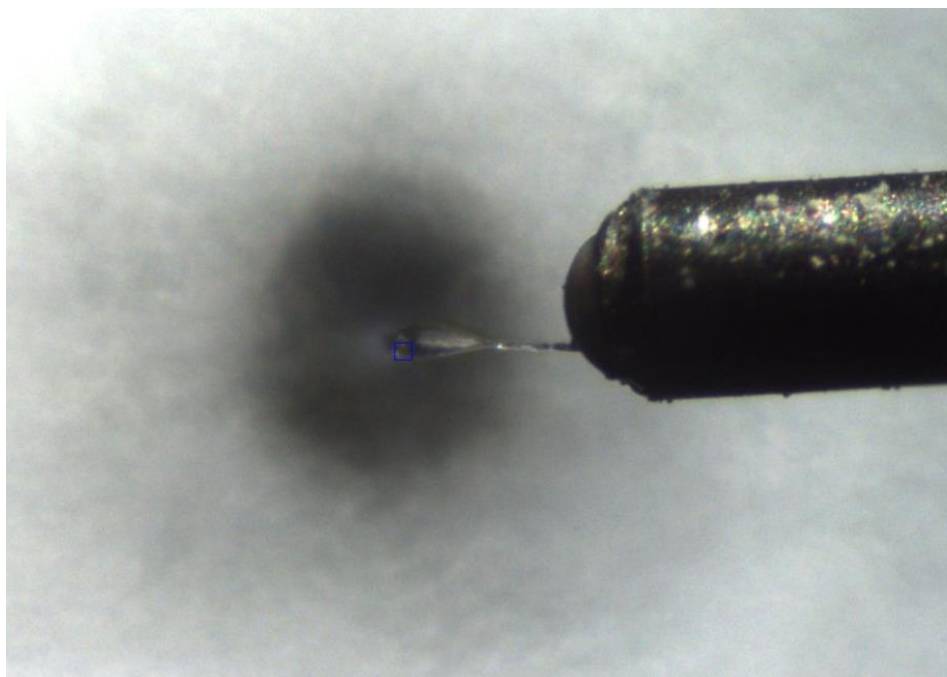


Figure 18. Image of crystal mounted in loop in front of detector with a small box outlining the actual crystal.

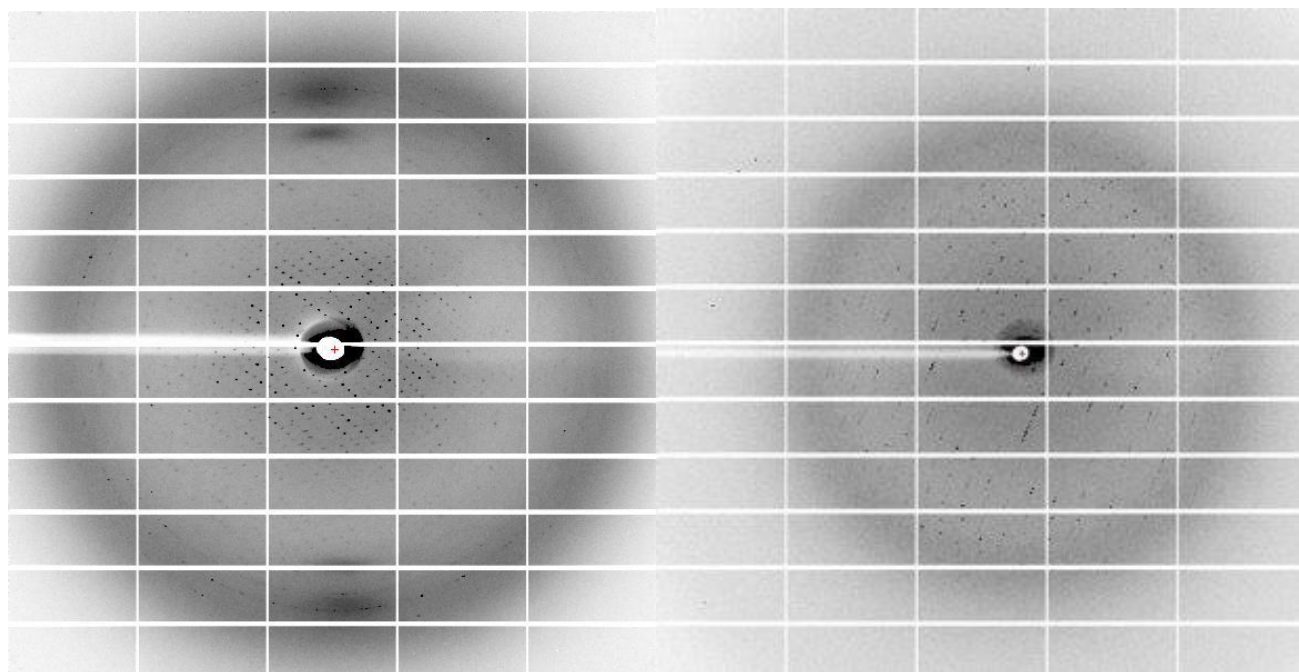


Figure 19. Diffraction data images for 2A9:Et3i and Til'E':Et3i complexes showing one of 165 diffraction images collected (image 67) for 2A9:FVIII complex (a) and one of 1442 diffraction images collected (image 4) for Til'E':FVIII complex (b).

After data collection, the diffraction images were processed using x-ray diffraction software (XDS).

This program takes all of the images, identifies spots which can be used, determines the space group and creates an unphased map of structure factors. Data processed by XDS is shown for the 2A9:Et3i complex in table 11 and for the Til'E':Et3i in table 12. It is notable that the 2A9:Et3i structure is 3.9 Å and is much lower resolution than the Til'E': Et3i structure at 2.8 Å.

Table 11. Processed diffraction data statistics from XDS program aimless.cc for 2A9:FVIII complex⁴²

aimless.cc summary	Overall	Inner Shell	Outer Shell
Low resolution limit	49.49	49.49	4.23
High resolution limit	3.92	10.37	3.92
Total number of observations	138780	7044	27991
CC(1/2)	0.992	0.998	0.329
Completeness	98.9	96.3	99.3
Average unit cell:	116.72 Å 116.72 Å 371.06 Å 90.00 90.00 90.00		
Space group:	P 4 ₁ 2 ₁ 2		
Average mosaicity:	0.22		

Table 12. Processed diffraction data statistics from XDS program aimless.cc for Til'E':FVIII complex

	Overall	Inner Shell	Outer Shell
Low resolution limit	48.42	48.42	2.87
High resolution limit	2.82	15.45	2.82
Total Number of Observations	673105	4014	32162
CC 1/2	0.992	0.996	0.306
Completeness	100.00	96.8	100.0
Average unit cell:	78.82 Å 136.12 Å 196.60 Å 90.00 99.90 90.00		
Space group:	P 1 2 ₁ 1		
Average mosaicity:	0.42		

Models Generated

From the processed diffraction data, a model was generated in PHENIX⁴³ for the 2A9:Et3i complex.

Using molecular replacement with a previously made model of Et3i⁴⁴ with the C2 domain deleted, an isolated C2 domain⁴⁵ and murine IgG2 α FAb 3E6.⁴⁶ The isolated C2 domain was used due to a difference in the conformation of C2 between the previous Et3i model and the crystal used to solve this structure. Fitting in the FAb required breaking it into two halves due to flexibility in the middle of the FAb. Iterative improvements in the model were made by building in the CDR loops of FAb 2A9, tweaking domain alignment, and editing orientation of individual residues utilizing COOT⁴⁷ and PHENIX. The final model of Et3i bound to 2A9 is shown below in figure 22.

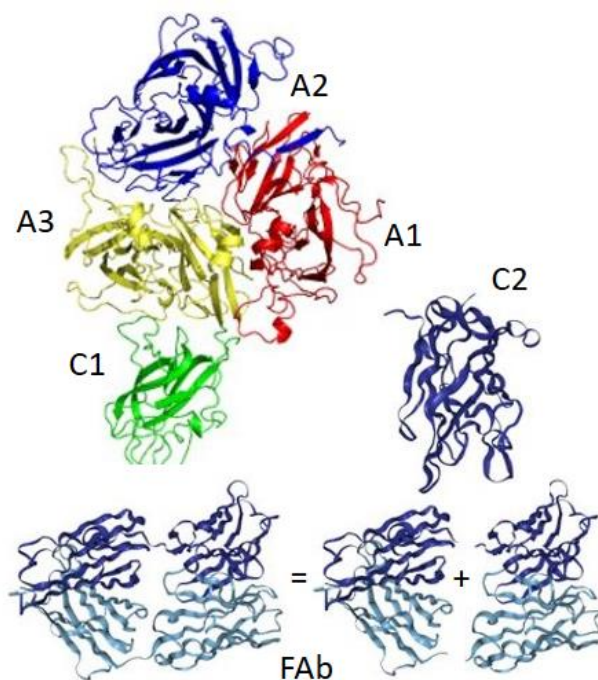


Figure 20. Molecular replacement solution strategy for the 2A9:Et3i complex

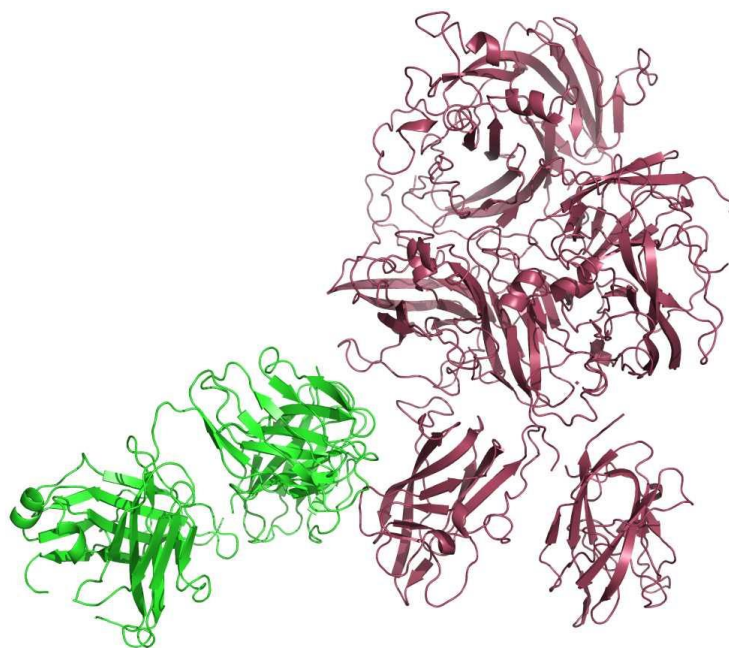


Figure 21. FVIII chimera Et3i (Raspberry) bound to FAb 2A9 (Green).

A molecular solution replacement using Et3i was readily achieved for the Til'E':Et3i complex. It was discovered that two copies of Et3i were a part of the structure. However, the Til'E' protein did not fit into the structure.

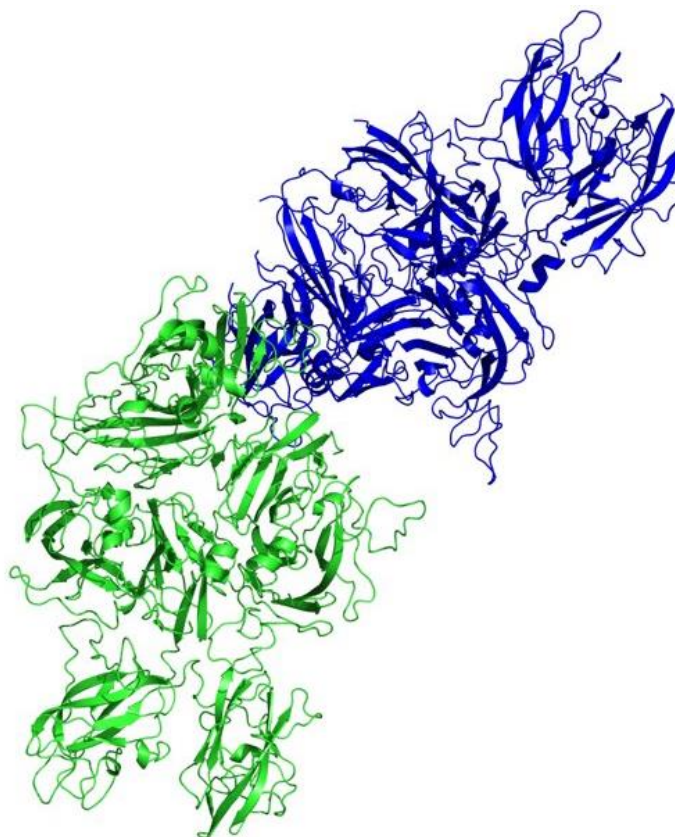


Figure 22. Working model of FVIII:Til'E' complex with a notable absence of Til'E' in the molecular replacement solution

Multiple rounds of refinement and adjusting models in PHENIX resulted in the current statistics for the models which are shown in table 13.

Table 13. Statistics for current models of structural complexes

paramter	2A9:Et3i	Til'E':Et3i
Resolution (Angstroms)	3.9	2.8
R-Work	0.24	0.23
R-Free	0.32	0.29

Atomic Interactions Between 2A9 and FVIII

When analyzing the structure of FAb 2A9 bound to FVIII, specific interactions can be seen which give rise to the high affinity interaction (0.9 nM).

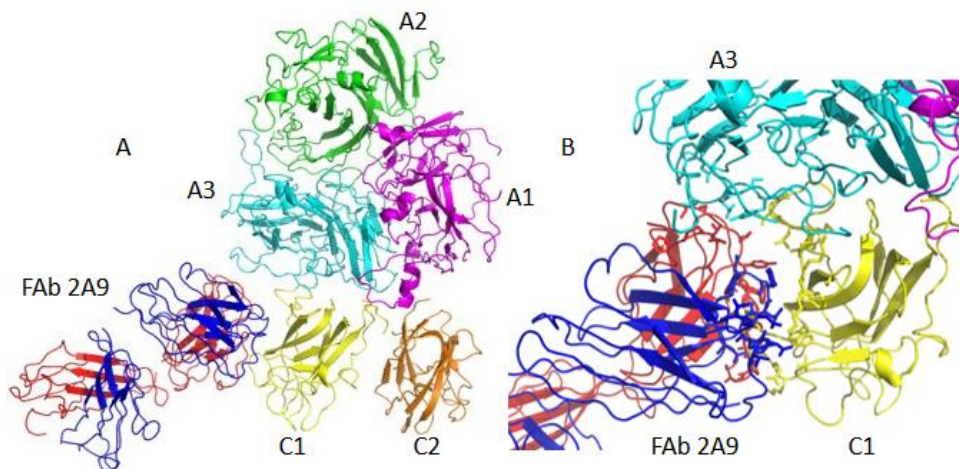


Figure 23. The interaction between FVIII and FAb 2A9 (A) showing stick models of interacting residues (B) (FAb 2A9 light chain: blue; heavy chain: red; FVIII C1: yellow; FVIII A3: cyan; FVIII A1: magenta). Of note, 2A9 appears to interact with both the C1 domain and the A3 domain of FVIII.

A loop on the side of the C1 domain, consisting of residues 2060-2070, was found to be the site of primary interactions. Phenylalanine 2068 on the C1 domain projects towards 2A9 and forms a nearly equilateral triangle with side lengths of 3.5 Å with F48 and F49 on the complementarity determining region of the heavy chain fragment of 2A9 (figure 24).

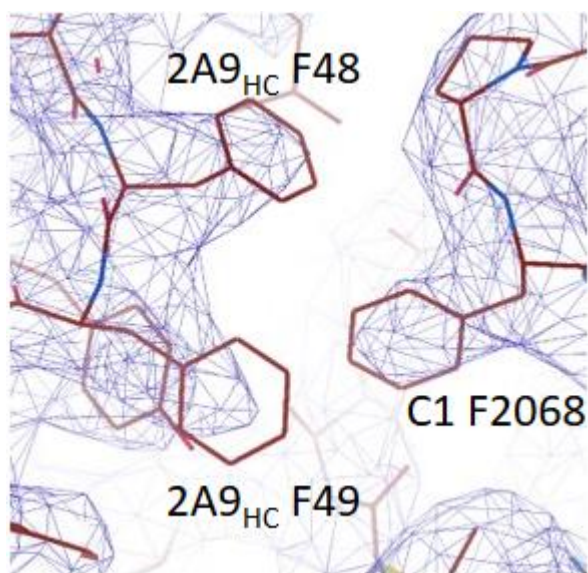


Figure 24. A hydrophobic interaction showing how F2068 on the C1 domain of Et3i interacts with F48 and F49 on the variable region of the heavy chain of FAb 2A9 (electron density map at 1.5 rmsd). 2A9_{HC} F48

On the same loop of residues 2060-2070 on the C1 domain of FVIII, W2070 formed a close contact with Y32 on the light chain of FAb 2A9.

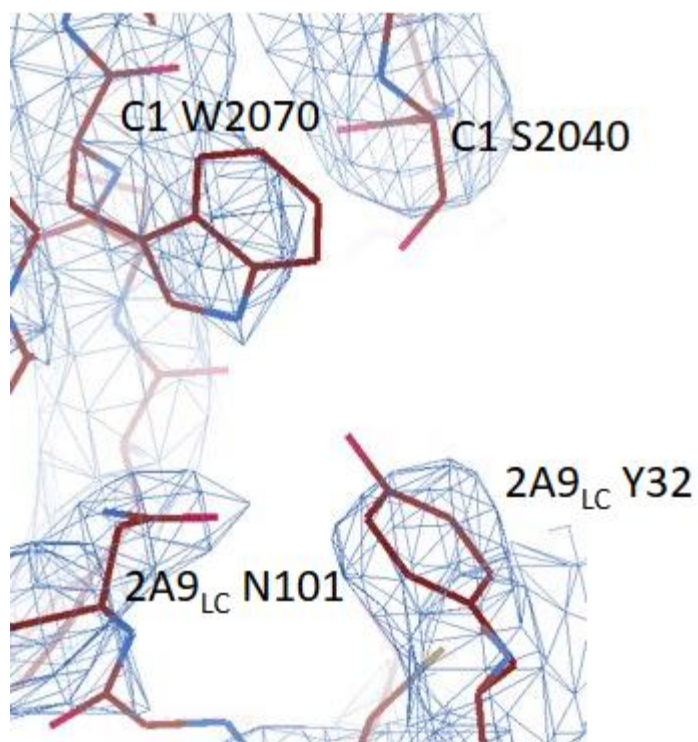


Figure 25. Tryptophan 2070 of the C1 domain interacts with Y32 and N101 on the light chain of 2A9 with S2040 of the C1 domain stabilizing the interaction (electron density map at 1.5 rmsd).

Another loop involved included H2155 of C1 which formed contacts with serine residues on the heavy chain of FAb 2A9.

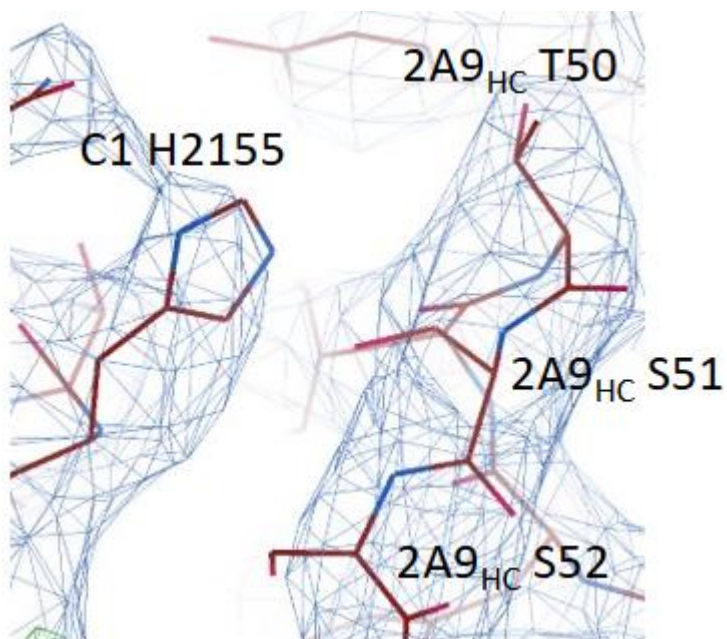


Figure 26. Intimate contacts between C1 domain H2155 and T50, S51, and S52 on the complementarity-determining region of the heavy chain of 2A9 (electron density map at 1.5 rmsd).

Interestingly, the A3 domain of FVIII also appears to be involved in the interaction between FVIII and FAb 2A9. Shown in figure 27, the loop on A3 including T1744 comes within 3.5 Å of S92 on the heavy chain of FAb 2A9.

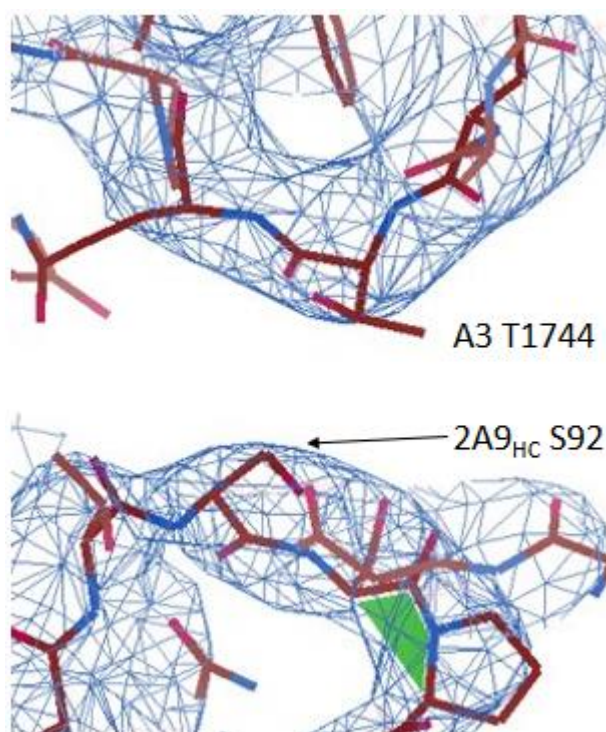


Figure 27. Interactions between T1744 of the A3 domain of FVIII and S92 of the heavy chain of 2A9 come within 3.5 Å (electron density map at 1.5 rmsd).

Discussion

Implications of FAb 2A9 Bound to Et3i for Understanding FVIII Mechanism

The structure of 2A9 bound to Et3i represents both the first structure of an anti-C1 domain structure bound to FVIII as well as the first structure of any antibody bound to a complete FVIII protein. Because a well established model for the interaction of FVIII exists, it is informative to note how the binding of inhibitory antibody 2A9 affects the physiological function of FVIII in light of this new structural data. The highest affinity sight of interaction appears to definitely be F2068 on the C1 domain of FVIII.

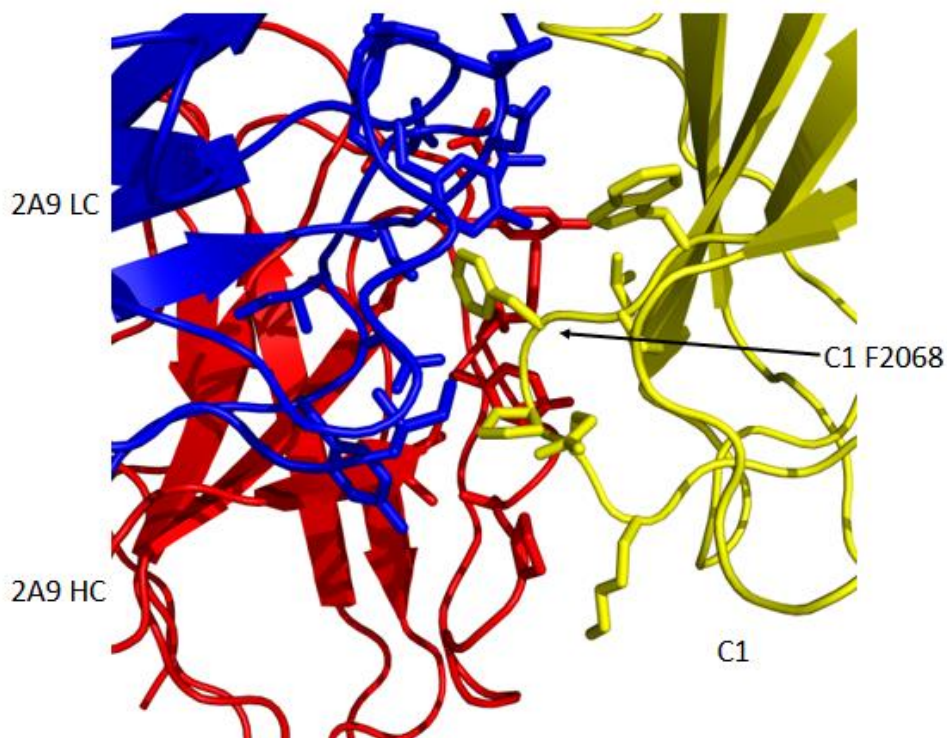


Figure 28. The site of interaction with the closest contacts is F2068 on the C1 domain of FVIII (FAb 2A9 light chain: blue; heavy chain: red; FVIII C1: yellow).

Previous characterization of IgG 2A9 determined that when 2A9 was bound to FVIII, it inhibited binding to phospholipid surfaces as well as vWF (table 3). This was determined by enzyme-linked immunosorbent assay (ELISA). Either vWF or PC:PS phospholipid vesicles were immobilized in wells. Next, FVIII which had been pre-incubated with 2A9 MAb was soaked in the well. Finally, a biotinylated anti-A1 MAb was placed in the well. After appropriate washing steps between each interval, an absorbance measurement was done at 405 nm to determine binding. It was determined that 2A9 successfully inhibited FVIII binding to vWF at 1.1 $\mu\text{g/ml}$ and phospholipid surfaces at 0.9 $\mu\text{g/ml}$.³⁹

In analyzing where vWF and the activated platelet surface bind to FVIII, it is apparent that 2A9 should interfere with the processes but does not directly block either of them. This reinforces the theory that antibodies which bind to FVIII will have a complex interaction with coagulation which can only be

determined by a Bethesda assay. It is possible to form antibodies against FVIII which are not detected because no physiological effect is seen.

Residues involved in 2A9:FVIII Interaction

The location of interaction between FVIII and 2A9 was predicted to be a loop of residues from 2060-2070 which is shown highlighted in figure 24 of the C1 domain based on mass-spectrometry data (figure 24). This was confirmed by the crystal structure produced in this study. It is interesting to note that the same loop of residues was found by negative-stain electron microscopy to be a primary site of interaction with the D'D3 region of vWF.

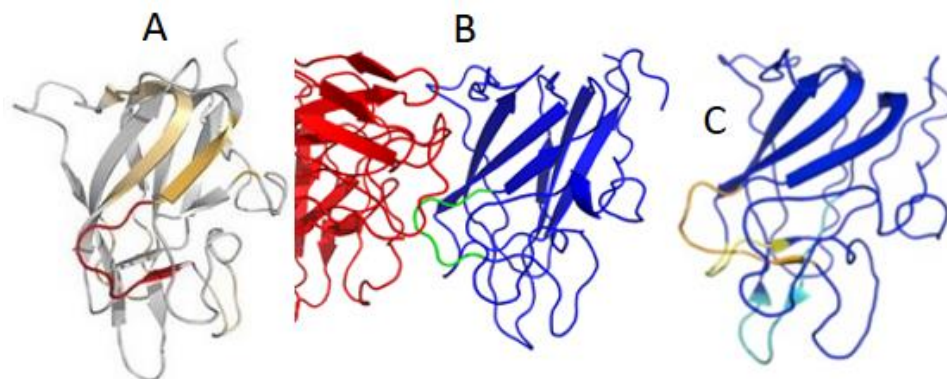


Figure 29. Interactions with loop 2060-2070 on C1 domain showing (A) binding region of 2A9 as determined by deuterium exchange, (B) binding interactions as determined by x-ray crystallography (residues 2062-2068 in green) (C) primary interaction site of vWF domains D'D3 with FVIII as determined by negative-stain electron microscopy.^{39,48}

Because antibody 2A9 does not inhibit vWF binding as strongly as antibody B136, which binds on the opposite side of the C1 domain (figure 25), it is reasonable to conclude that residues 2060-2070 do not comprise the high affinity site, but rather are involved in the vWF interaction. More likely, the C1 domain must undergo a conformational shift in order to facilitate vWF binding. This would explain why B136 inhibits vWF binding much more strongly than 2A9 and corroborates with the hypothesis put forward by Yee *et. Al.* (10) which posits a significant shift in the packing of the C1 domain in order to facilitate the binding of D'D3 based on cryo-EM data.



Figure 30. Antibody B136 epitope on C1 domain of FVIII shown in red.³⁹

It is interesting to note that Et3i appears to interact with 2A9 via the A3 domain as well as the C1 domain (figure 27). This interaction was not previously reported and could contribute to reduced mobility of the C1 domain upon activation. In this case, it appears that C1 is not able to adopt a favorable conformation for membrane binding which is why 2A9 interferes with phospholipid binding.

Glycosylation on Arginine 2118 of FVIII is part of Epitope

Investigating the structure of 2A9 bound to FVIII reveals that glycosylation of arginine 2118 is near the epitope recognized by 2A9. This is significant because glycosylation of FVIII therapeutics is an important factor in determining immunogenicity.

To introduce a caveat, it is important to note that this model is 3.9 Angstrom resolution, and just because sugar is present near the binding site of 2A9 does not mean it is necessarily epitopically involved in binding. The sugar molecules have not been able to be built into the structure due to the low resolution of the structure. However, as was noted in the introduction, post-translational modifications, such as glycosylation, of FVIII therapeutics do contribute to immunogenicity.

Co-Crystallization of Et3i and Til'E'

While attempting to make crystals of Et3i complexed to Til'E', the highest resolution to date structural information on FVIII has been collected. It remains to be seen if this actually is a crystal of the complex, but a simple kinetics solution to encourage binding could be accomplished by increasing the molar ratio of Til'E' to Et3i. In the past, other groups have noted a wide range of affinity values of the D' region of FVIII. These range from 3 nM to micromolar. For Til'E', reported values include 26 nM as measured by ELISA and 330 nM as measured by ITC. The off-rate for truncated Til'E' has also been noted to be greater than that for vWF. Because of this, it may be useful to increase the molar ratio of Til'E' to Et3i from 1.2:1 to 10:1.

The absence of Til'E' could also be due to the high magnesium nitrate concentration (200 mM) used for crystallization. If this interferes with the interaction, it is possible that this crystallization condition is not going to result in a solution of the structure of Til'E' bound to FVIII. It would be worthwhile to test how the interaction changes depending on magnesium nitrate concentration as well as attempting to grow crystals with a lower magnesium nitrate concentration.

When observing the supposed binding region of Til'E' to FVIII in the dataset which was collected, it is obvious that there is an apparent lack of electron density.

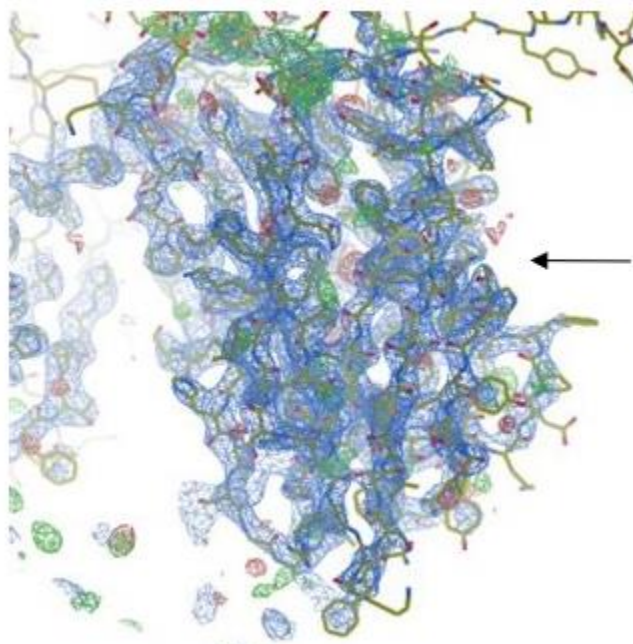


Figure 31. A lack of electron density in the putative binding region of vWF on the C1 domain of FVIII indicated by blank space at tip of arrow.

Potential Problems with Molecular Replacement Solutions using Til'E' Structure

When attempting a molecular replacement solution of the Til'E' domain which is allegedly bound to Et3i in the crystals grown, the 2.5 Angstrom resolution Til'E' domain from PDB ID: 6N29 was used.

When analyzing this structure, it is interesting to note that the electron density at 1.5 RMSD is notably absent from the region suspected of binding with FVIII. It is possible that these residues are inherently flexible and only lock in to place when vWF is bound to FVIII. In this case, the actual residues will have to be built in manually to solve the structure.

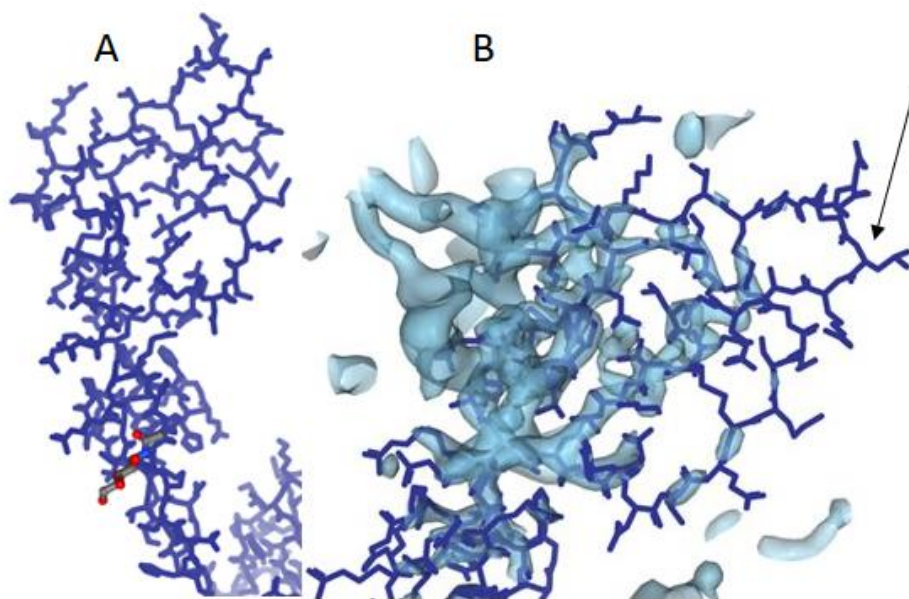


Figure 32. Model of Til'E' from PDB ID: 6N29 (A) and electron density map superimposed on model with an arrow pointing to the high-affinity interaction residues based on previous models (B).

Assessing Quality of Model

Thus far I have examined the implications of the model I have created showing Et3i in complex with antibody 2A9 FAb. It would be a gross oversight to not analyze the quality of the model in order to understand its inherent limitations.

Resolution of a crystallographic model is based on the distance which spots (called reflections) are diffracted from the beam on the detector. Each reflection represents a structure factor. The resolution of a structure depends on how many structure factors are present in an inverse cube manner. Therefore, a 1 Angstrom resolution structure has twenty-seven times more structure factors than a 3 Angstrom resolution structure. The resolution limit of the Et3i:2A9 complex is 3.9 Angstroms. This is therefore a low-resolution structure. Exact conformations of side chains and loops are suspect. However, because this same class of antibody has been crystallized before, and FVIII has been crystallized before, it is reasonable to accept this structure as a reasonable solution.

The r-values (r-free and r-work) of a structure are interpreted as a goodness of fit of the structure factors which are calculated versus those which are observed. The r-free value is based on “withholding” 10% of reflections from model refinement. These withheld values are checked against further rounds of refinement. A wide divergence between r-work (which uses the 90% of reflections used to calculate structure) and r-free indicates overfitting of the model. As a rule of thumb, an r-free value of one tenth of the resolution limit is appropriate to a model. Since the resolution is 3.9 Angstroms, the r-free of 0.34 for this structure is perfectly acceptable. The r-work value of 0.27 does not represent a wide divergence from the r-free.

Less than ninety degrees of rotation were used to solve this structure. This was because x-ray radiation was damaging the crystal due to a long exposure time necessary to measure the reflections on the detector. Each exposure was three seconds long, so by the time the crystal had made it ninety degrees, it began rapidly losing structure factors. Attempting to solve the structure using data from the degraded crystal would have dramatically decreased the resolution.

Discussion on Murine versus Human Antibody Response

It should be noted that antibody 2A9 was generated by injecting FVIII into a mouse and harvesting B-cells which produced antibodies against FVIII. As such, 2A9 is a murine antibody and the question naturally arises, what significance does this have for the human antibody response against FVIII?

Importantly, despite differences in the innate immune system and the exact classes of IgG expressed, the generated antibodies are essentially identical. The most significant difference is in the Fc region of the antibody. However, in this crystallographic study, the Fc region has been removed, so the difference is not important.⁴⁹

Although the response was generated in a mouse model, it still provides information as to how antibodies can affect FVIII function because human inhibitory antibodies frequently target the C1 domain. Knowing the exact binding interaction of 2A9 to FVIII and seeing how this affects platelet binding as well as vWF binding informs understanding of FVIII physiological function.

Notes on Preparation of Antigen Binding Fragments (FABs)

Preparation of an FAb from a monoclonal antibody is supposed to be a very straightforward process. In theory, enzyme and substrate are mixed in a pre-determined ratio and the reaction proceeds according to set parameters which result in successful cleavage of the antibody and an easily purified product. This simple process, as shown in figure 29, proved to be very difficult to accomplish. Seeking to understand why will hopefully ease the pain for would-be cleavers who read this.

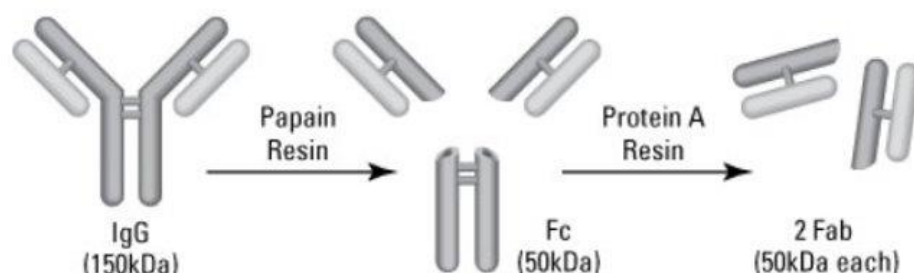


Figure 33. Cleavage of monoclonal antibody to make FAb.

The first step is to break down the process into each possible variable and address in-depth what could have gone wrong before drawing conclusions.

To begin with, reagent quality is of primary importance. Steps to ensure this are to properly store chemicals, make fresh buffers which are filtered to 0.2 micron, and to avoid contamination at all steps with enzymes, bacteria, etc. The enzyme which does the actual cleaving should be prepared properly.

Generally, these enzymes are agarose-linked and stored with azide. It is crucial that the agarose is not allowed to dry out and that the residual azide is washed away by equilibrating the enzyme in reaction buffer. Reaction buffer must contain cysteine in order to prep the enzyme and generate full FAbs. An insufficient concentration of cysteine will doom the reaction to failure. The enzyme to substrate ratio is a huge variable. According to product information, a ratio of 1:10 to 1:160 may be appropriate for papain cleavage of MAbs. It is best to try a range of concentrations in a test cleavage reaction to ensure that enough but not too much enzyme is used.

Purity of the antibody to be cleaved is essential to obtain a successful cleavage reaction. My first cleavage attempts were on antibody that had been purified by ion exchange chromatography. This was not pure protein in that the A_{260}/A_{280} ratio was relatively high at around 0.7. Further trials after protein A+ purification dropped the A_{260}/A_{280} ratio to very close to an ideal value of 0.5, this enabled consistent cleavage.

Concentration of the antibody to be cleaved is proportional to the efficiency of the reaction. Low concentration reactions do work, but more enzyme per substrate must be used. This increases the cost.

The final variable is ensuring proper mixing of enzyme and substrate during the cleavage reaction. Because Papain is agarose linked, it settles out of solution in a matter of seconds. For an overnight cleavage reaction, reaction volume and enzyme quantity are key variables which affect the mixing rate needed. There are several strategies which may work. For the preparation of 2A9 FAb, the reaction was mixed at 260 RPM in a 1.5 mL Eppendorf tube secured horizontally in benchtop shaker at 37° C overnight. Lower RPMs were not sufficient to keep agarose resin in constant mixing. An alternative strategy would be to place the reaction vessel in a beaker of water at 37° C on a stirring hot plate with a magnetic stir bar maintaining constant mixing of the reaction.

To conclude this discussion of antibody cleavage, I attempted the reaction at least twelve times, and the specific variables I made mistakes on are outlined in table 14 below.

Table 14. Papain cleavage errors

Actual Errors I made	Result
Old/degraded Papain	No Cleavage
Non-pure Antibody Sample	No Cleavage
Low-concentration cysteine digestion buffer	No Cleavage
Improper buffer exchange of antibody into sample buffer	No Cleavage
Insufficient mixing of agarose-linked papain during cleavage	No Cleavage
Too Low of reaction temperature	No Cleavage
Too low of enzyme:substrate ratio	No Cleavage
Contaminated Buffers	No Cleavage
Not washing residual azide from agarose-linked papain	No Cleavage

Notes on Crystallization Strategies

There were a number of unique strategies employed to optimize crystal growth. While none of these techniques were entirely original, a compilation of these methods here may serve to assist future crystallographers achieve their dreams.

The first strategy to find a lead was sending a 500 μ l sample to the Hauptman-Woodward Institute. They have a high-throughput process which enables screening of 1536 conditions for less than five hundred dollars. To do this operation in-house would require the preparation of 1536 conditions, use of 64 plates, at very minimum 1.5 ml of sample, and several weeks of labor. This makes utilization of a screening service both a cost-saving measure and an indispensable first step towards obtaining an appropriate crystallization condition.

Upon obtaining a lead condition, a wide screen should first be conducted where pH and precipitant concentration are varied. Varying pH in one-half unit increments and precipitant by two percent

surrounding the initial hit is a good strategy. When using polyethylene glycol as a precipitant, it is useful to try different molecular weight PEGs due to the differential effects on protein stability.

When preparing a set of crystallization conditions, far more intra-tray consistency can be achieved by preparing only four conditions instead of twenty-four. These four conditions represent the extrema on the x- and y-axis. By appropriately mixing them together with a multi-channel pipette in the tray, a complete set of conditions can be made in a matter of minutes. This provides the ability to screen conditions of PEG with much greater certainty due to frequent errors which can occur when pipetting high molecular weight PEGs.

Once a particular pH or PEG concentration is discovered which reliably produces crystals, it can be useful to turn the tray into a one variable experiment. To accomplish this, two tubes (A and B) are prepared which are identical except for, as an example, PEG concentration. Tube A is pipetted into wells 1-24 at a steadily decreasing rate such that well 1 is 100% tube A and well 24 is 0% tube A. Tube B is pipetted in a converse manner such that all wells have the same final volume and a smooth gradient of the variable being queried. The in-well mixed conditions should be allowed to mix by shaking at 200 RPM for at least 15 minutes to ensure proper preparation and to achieve consistent results.

A further refinement is varying well volume. Total well volume of crystallization trays is a maximum of about 1200 μ l to allow room for the hanging drop to not come into contact with the reservoir. Varying this volume from 1200 to 0 μ l has a dramatic effect on how quickly the drop dehydrates to an effective crystallizing condition. Theoretically, a greater well volume will increase the rate of exchange of water molecules between the drop and mother liquor. Whether this is due to a proximity effect (the surface of the mother liquor is physically closer to the drop) or to a larger volume pulling liquid faster is not known at this time. This phenomenon is certainly worthy of further investigation.

Conclusion

Final Notes on inhibitors

As introduced in the beginning of this thesis, the formation of inhibitors to FVIII is a complicated phenomenon which cannot be readily predicted. Knowledge of atomic level interactions of inhibitors against FVIII help us gain more information as to how FVIII behaves physiologically as well as providing information on how to engineer a less immunogenic protein.

Final Notes on FVIII:Til'E' Complex

To date, atomic resolution data has been provided for b-domain deleted FVIII and the D'D3 of von Willebrand Factor. The information derived from these structures provides a nearly complete picture of the interaction between FVIII and vWF. However, the final structure at 2.8 Å resolution may be sitting on my computer right now, and if not, is hopefully within the grasp of the Spiegel lab.

Future Work

Research into improved treatments for hemophilia A should continue until the disease can be fully eradicated through gene therapy means. Seeing as that a cure of such nature is not currently foreseeable, continuing to provide information on the basic physiological function of FVIII in order to engineer FVIII therapeutics with reduced immunogenicity should continue to be a priority for hemophilia A research.

Works Cited

1. "Coagulation." *Merriam-Webster.com*. Merriam-Webster, 2019. Web. 30 July 2019.
2. Versteeg, Henri H., et al. "New fundamentals in hemostasis." *Physiological reviews* 93.1 (2013): 327-358.
3. World Federation of hemophilia, accessed 5/2019
4. Online source: <http://eclinpath.com/hemostasis/physiology/secondary-hemostasis/coagulation-cascade-new-model-3/> accessed: August 2019
5. Lenting, Peter J., Jan A. van Mourik, and Koen Mertens. "The life cycle of coagulation factor VIII in view of its structure and function." *Blood* 92.11 (1998): 3983-3996.) (Gitschier, Jane, et al. "Characterization of the human factor VIII gene." *nature* 312.5992 (1984): 326.)
6. Shen, Betty W., et al. "The tertiary structure and domain organization of coagulation factor VIII." *Blood* 111.3 (2008): 1240-1247
7. Gitschier, Jane, et al. "Genetic basis of hemophilia A." *Thrombosis and haemostasis* 65.01 (1991): 037-039.
8. Monroe DM, 3rd, Hoffman M, Roberts HR. Williams Hematology. 8th ed. New York NY: McGraw-Hill Professional Publishing; 2010. Molecular biology and biochemistry of the coagulation factors and pathways of hemostasis; pp. 614–6.
9. Vlot, A. J., et al. "Kinetics of factor VIII-von Willebrand factor association." *Blood* 87.5 (1996): 1809-1816.
10. Yee, Andrew, et al. "Visualization of an N-terminal fragment of von Willebrand factor in complex with factor VIII." *Blood* 126.8 (2015): 939-942.
11. Sadler, J. Evan. "Biochemistry and genetics of von Willebrand factor." (1998): 395-424.

12. Foster, Paul A., et al. "A major factor VIII binding domain resides within the amino-terminal 272 amino acid residues of von Willebrand factor." *Journal of Biological Chemistry* 262.18 (1987): 8443-8446.
13. Przeradzka, Małgorzata A., et al. "The D' domain of von Willebrand factor requires the presence of the D3 domain for optimal factor VIII binding." *Biochemical Journal* 475.17 (2018): 2819-2830.
14. Leyte, A.; Schijndel, H. B. van; Niehrs, C.; Huttner, W. B.; Verbeet, M. P.; Mertens, K.; Mourik, J. A. van (1991-01-15). "Sulfation of Tyr1680 of human blood coagulation factor VIII is essential for the interaction of factor VIII with von Willebrand factor". *Journal of Biological Chemistry*. 266 (2): 740–746. ISSN 0021-9258. PMID 1898735
15. Online source:
<https://patentimages.storage.googleapis.com/ae/cd/6e/58959196e88578/US20160120954A1.pdf>
accessed: August 2019
16. Shiltagh, Nuha, et al. "Solution structure of the major factor VIII binding region on von Willebrand factor." *Blood* 123.26 (2014): 4143-4151.
17. Chow, Thomas W., et al. "Shear stress-induced von Willebrand factor binding to platelet glycoprotein Ib initiates calcium influx associated with aggregation." *Blood* 80.1 (1992): 113-120.
18. Pittman, Debra D., and Randal J. Kaufman. "Proteolytic requirements for thrombin activation of anti-hemophilic factor (factor VIII)." *Proceedings of the National Academy of Sciences* 85.8 (1988): 2429-2433.
19. Lü, Junhong, et al. "A membrane-interactive surface on the factor VIII C1 domain cooperates with the C2 domain for cofactor function." *Blood* 117.11 (2011): 3181-3189.

20. Gilbert, Gary E., Barbara C. Furie, and Bruce Furie. "Binding of human factor VIII to phospholipid vesicles." *Journal of Biological Chemistry* 265.2 (1990): 815-822.
21. Lenting, P. J., et al. "Identification of a binding site for blood coagulation factor IXa on the light chain of human factor VIII." *Journal of Biological Chemistry* 269.10 (1994): 7150-7155.
22. Saenko, Evgueni L., et al. "Role of the low density lipoprotein-related protein receptor in mediation of factor VIII catabolism." *Journal of Biological Chemistry* 274.53 (1999): 37685-37692.
23. Sarafanov, Andrey G., et al. "Identification of coagulation factor VIII A2 domain residues forming the binding epitope for low-density lipoprotein receptor-related protein." *Biochemistry* 45.6 (2006): 1829-1840.
24. Bovenschen, N., et al. "The B domain of coagulation factor VIII interacts with the asialoglycoprotein receptor." *Journal of Thrombosis and Haemostasis* 3.6 (2005): 1257-1265.
25. van Schooten, Carina J., et al. "Macrophages contribute to the cellular uptake of von Willebrand factor and factor VIII in vivo." *Blood* 112.5 (2008): 1704-1712.
26. Lakich, Delia, et al. "Inversions disrupting the factor VIII gene are a common cause of severe haemophilia A." *Nature genetics* 5.3 (1993): 236.
27. Cafuir, Lorraine A., and Christine L. Kempton. "Current and emerging factor VIII replacement products for hemophilia A." *Therapeutic advances in hematology* 8.10 (2017): 303-313.
28. Lieuw, Kenneth. "Many factor VIII products available in the treatment of hemophilia A: an embarrassment of riches?." *Journal of blood medicine* 8 (2017): 67.
29. Janeway Jr, Charles A., et al. "B-cell activation by armed helper T cells." *Immunobiology: The Immune System in Health and Disease. 5th edition*. Garland Science, 2001.

30. Astermark, Jan. "Why do inhibitors develop? Principles of and factors influencing the risk for inhibitor development in haemophilia." *Haemophilia* 12 (2006): 52-60.
31. Hermeling, Suzanne, et al. "Structure-immunogenicity relationships of therapeutic proteins." *Pharmaceutical research* 21.6 (2004): 897-903.
32. Lee, Christine A., David Lillicrap, and Jan Astermark. "Inhibitor development in hemophiliacs: the roles of genetic versus environmental factors." *Seminars in thrombosis and hemostasis*. Vol. 32. No. S 2. Copyright© 2006 by Thieme Medical Publishers, Inc., 333 Seventh Avenue, New York, NY 10001, USA., 2006.
33. Oldenburg J, Pavlova A (2006) Genetic risk factors for inhibitors to factors VIII and IX. *Haemophilia* 12(Suppl 6):15–22
34. Zhang, Ai Hong, Jonathan Skupsky, and David W. Scott. "Factor VIII inhibitors: risk factors and methods for prevention and immune modulation." *Clinical reviews in allergy & immunology* 37.2 (2009): 114-124.
35. Fakharzadeh SS, Kazazian HH Jr. Correlation between factor VIII genotype and inhibitor development in hemophilia A. *Semin Thromb Hemostasis* 2000; 26: 167–171
36. Carpenter, John F., et al. "Overlooking subvisible particles in therapeutic protein products: gaps that may compromise product quality." *Journal of pharmaceutical sciences* 98.4 (2009): 1201-1205.
37. Rebecca Kruse-Jarres MD, MPH, Cindy A. Leissinger MD, in *Consultative Hemostasis and Thrombosis (Third Edition)*, 2013
38. Healey JF, Parker ET, Barrow RT, Langley TJ, Church WR, Lollar P. The humoral response to human factor VIII in hemophilia A mice. *J Thromb Haemost*. 2007;5(3):512-519.

39. (Batsuli, Glaivy, et al. "High-affinity, noninhibitory pathogenic C1 domain antibodies are present in patients with hemophilia A and inhibitors." *Blood* 128.16 (2016): 2055-2067.)
40. Doering, C. B.; Healey, J. F.; Parker, E. T.; Barrow, R. T.; Lollar, P. Identification of Porcine Coagulation Factor VIII Domains Responsible for High Level Expression via Enhanced Secretion. *Journal of Biological Chemistry* 2004, 279(8), 6546–6552.
41. Luft, J. R., Collins, R. J., Fehrman, N. A., Lauricella, A. M., Veatch, C. K. & DeTitta, G. T. (2003). A deliberate approach to screening for initial crystallization conditions of biological macromolecules. *J. Struct. Biol.* 142, 170-179.
42. Data collected by Rachel Werther, March 2019
43. PHENIX: a comprehensive Python-based system for macromolecular structure solution. P. D. Adams, P. V. Afonine, G. Bunkóczi, V. B. Chen, I. W. Davis, N. Echols, J. J. Headd, L.-W. Hung, G. J. Kapral, R. W. Grosse-Kunstleve, A. J. McCoy, N. W. Moriarty, R. Oeffner, R. J. Read, D. C. Richardson, J. S. Richardson, T. C. Terwilliger and P. H. Zwart. *Acta Cryst. D* 66, 213-221 (2010).
44. Smith, Ian. "Structural Characterization of a Human/Porcine Chimeric FVIII Construct and an Improved Human Factor VIII Model and Progress Towards Determination of the FVIII C1 Domain In Complex With Inhibitory Antibodies." (2018).
45. Pratt, Kathleen P., et al. "Structure of the C2 domain of human factor VIII at 1.5 Å resolution." *Nature* 402.6760 (1999): 439.
46. Wuerth, Michelle E., Rebecca K. Cragerud, and P. Clint Spiegel. "Structure of the human factor VIII C2 domain in complex with the 3E6 inhibitory antibody." *Scientific reports* 5 (2015): 17216.

47. Emsley, Paul, et al. "Features and development of Coot." *Acta Crystallographica Section D: Biological Crystallography* 66.4 (2010): 486-501.
48. Chiu, Po-Lin, et al. "Mapping the interaction between factor VIII and von Willebrand factor by electron microscopy and mass spectrometry." *Blood* 126.8 (2015): 935-938.
49. Mestas, Javier, and Christopher CW Hughes. "Of mice and not men: differences between mouse and human immunology." *The Journal of Immunology* 172.5 (2004): 2731-2738.

Appendix

Spectra BR Ladder was used for SDS-PAGE analysis

A Spectra BR ladder was used for all SDS-PAGE analysis. The ladder consists of 10 bands which are shown below in figure A1. For more information: Thermo Scientific Spectra Multicolor Broad Range Protein Ladder Pub. No. MAN0011774 Rev. Date 19 June 2019 (Rev. C.00) Thermo-Scientific product number: 26623

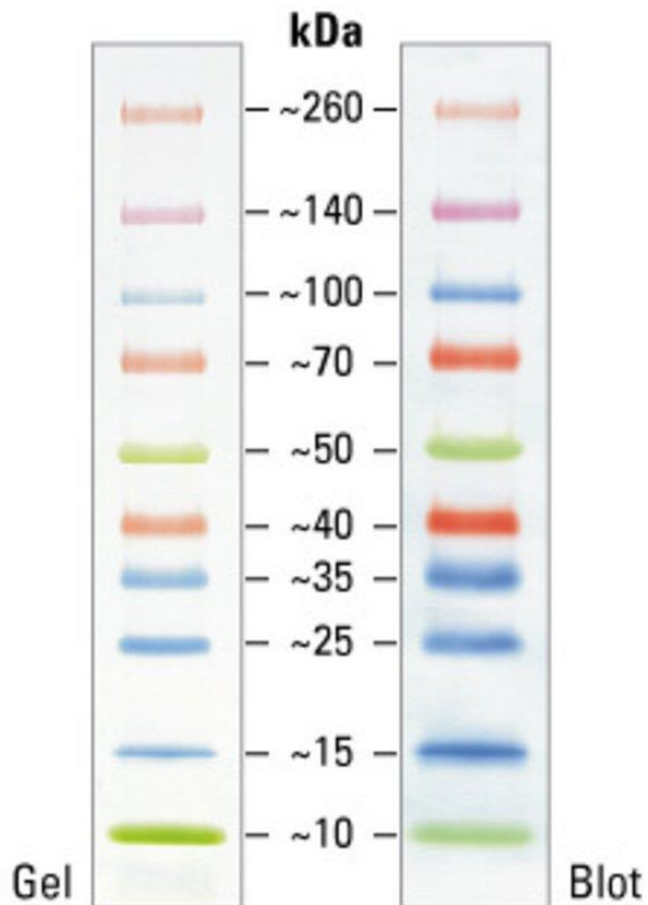


Figure A1. Spectra BR ladder showing standard molecular weights in kDa.

Further Note on Crystallization Strategy

An alternative to attempting to create the exact right crystallizing condition and allowing the drop to gradually change size is salt titration crystallization. In this technique, a well is prepared which is known to not result in crystallization. The drop is allowed to equilibrate with the mother liquor after it is sealed in. At this point, a concentrated salt solution is added periodically to the mother liquor and the well is carefully resealed to prevent moisture from the air entering the crystallization chamber. The hygroscopic effect of continual salt addition results in temporal control of crystallization. The faster salt is added, the faster the precipitation will occur and vice versa. The most important aspect of this technique is that the protein to be crystallized is entirely stable after reaching equilibrium with the mother liquor prior to any salt additions. As an example, periodic addition of 5 μ l of 5 M NaCl to a 400 μ l well would result in the following increase in NaCl molarity (rounded): 0 mM, 60 mM, 120 mM, 180 mM, 240 mM, 300 mM. Considering the massive effect in pressure this has, the potential for exquisite control of crystallization is limited only by the crystallographers imagination.

Immobilized Metal Affinity Chromatography

A useful tool for purifying proteins for biochemical studies is immobilized metal affinity chromatography (IMAC). The affinity resin contains a positively charged metal linked to beads such as nickel. An affinity tag is engineered into the protein sequence of six histidine residues in a row. This HIS₆ tag binds tightly to the resin and can be used to easily purify proteins in a single step. Purification can be accomplished by either allowing the resin to settle and then passing the media containing protein over it, or “batch” style where resin is pre-incubated in a container with the media and then poured over the column. The resin is then washed until a stable OD₂₈₀ reading is achieved before eluting the bound protein with a high concentration of imidazole (generally 150 mM).

Variable Region cDNA Sequence Analysis of 2A9 Antibody

NOTE: This section is all text directly from Green Mountain Antibodies report and is presented here as supplemental information.

2A9 Heavy Chain DNA Sequence of variable region and complementarity determining region.

cagatccagttggtgcagctctggacctgagctgaagaagcctggagagacagtcaagatctctgcaaggctcttggtataccttcacagactattcaatgactgggtgaagcaggctccaggaaaggggttaagtggatgggctggataaacactgagactggtgagccaacatatgcagatgacttcaagggacggtttgccttctctttgaaacctctgccagctctgcctatttgcagatcaacaacctcaaaaatgaggacacggctacatatttctgtgctagatgcggt aactacgtggactatgctatagactactggggcaaggaacctcagtcaccgtctcttcag

Predicted Protein Sequence

Complementarity determining regions (CDRs) are underlined.

QIQLVQSGPELKKPGETVKISCKASGYTFTDYSMHWVKQAPGKGLKWMGWINTETGEPTYAD
DFKGRFAFSLETSASSAYLQINNKNEDTATYFCARCGNYVDYAIDYWGQGTSTVTVSS

2A9 Light Chain DNA Sequence of variable region and complementarity determining region.

gaaaatgtgctcaccagctctccagcaatcatgtctgcatctctaggggagaaggctcaccatgagctgcagggccacctcaagtgtaaattacatgtatt ggtaccagcagaagtcagatgcctccccaaactatggattttttcacatccagcctggctcctggagtcccagctcgttcagtggcagtggtctgg gaactcttattctctcacaatcagcagcgtggagggtgaagatgctgccacttattactgccagcagtttactagttccctttcacgttcggctcggggac aaagctggaaatcaaac

Predicted Protein Sequence

Complementarity determining regions (CDRs) are underlined.

ENVLTQSPAIMASLGEKVTMSCRATSSVNYMYWYQQKSDASPKLWIFFTSSLAPGVPARFSGS
 GSGNSYSLTISSVEGEDAATYYCQQFTSSPFTFGSGTKLEIK

Sample Preparation

Total RNA was isolated from the hybridoma cell line culture (2 x 10⁶ cells). RNA was treated to remove aberrant transcripts and reverse transcribed using oligo(dT) primers. Samples of the resulting cDNA were amplified in separate PCRs using framework 1 and constant region primer pairs specific for either the heavy or light chain. Reaction products were separated on an agarose gel, size-evaluated and recovered. In some cases, a second, nested PCR is performed to increase yield of the desired fragment(s). Amplicons were cloned into pCR®4-TOPO vector using the TA cloning strategy. 12 colonies were selected and plasmid DNA was amplified using primers specific for vector DNA sequences. PCR product size for each cloned insert was evaluated by gel electrophoresis, and 6 reactions were prepared for sequencing using a PCR clean up kit and sequenced at the Dartmouth College Molecular Biology & Proteomics Core Facility using cycle sequencing with fluorescent dye terminators and capillary-based electrophoresis.

Table A1. Project specifications for antibody sequencing.

	Heavy Chain	Light Chain
Clones sequenced	4	5
Clones with >98% DNA sequence-identity	4	5
Consensus DNA sequence is consistent with murine immunoglobulin sequence	yes	yes

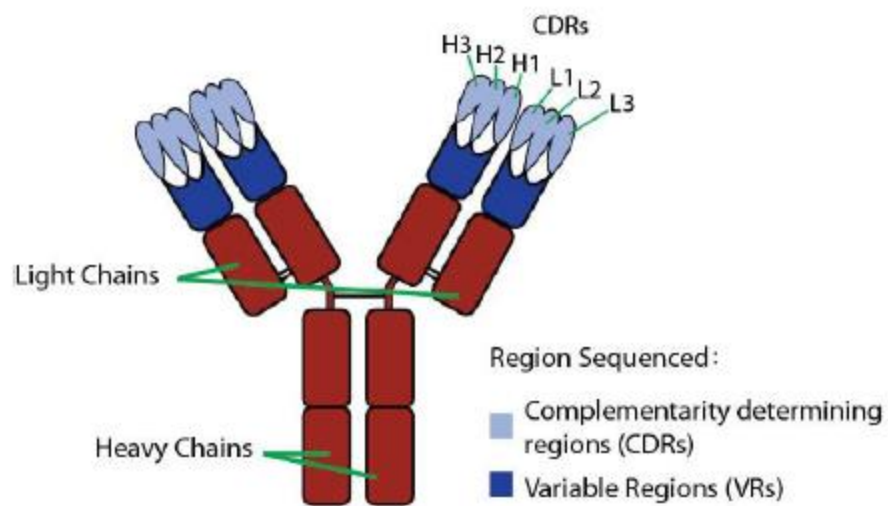


Figure A2. Locations on antibody 2A9 which were sequenced.